

Review

Lidar studies of the polar troposphere

Graeme J. Nott* and Thomas J. Duck

Department of Physics and Atmospheric Science, Dalhousie University, Halifax, Nova Scotia B3H 4R2, Canada

ABSTRACT: The lidar is a widely-used remote sensing tool for measurements of tropospheric constituents and processes. Despite considerable operational challenges, lidars have been deployed in the polar regions to study the unique characteristics of the high-latitude atmosphere. The relevant technologies and techniques used for profiling the polar troposphere are reviewed. Lidars and their measurements are described, from the first single-wavelength lidar aircraft campaign to today's multiple-wavelength, multiple-data product systems and satellite-borne lidars providing large-area polar coverage. Significant advancements in our understanding of tropospheric aerosols, clouds, structure, and trace gases in both the Antarctic and Arctic have been made possible through the use of lidars and these will be discussed. Copyright © 2011 Royal Meteorological Society

KEY WORDS Arctic; Antarctic; aerosols; clouds; water vapour; ozone

Received 19 May 2011; Revised 25 July 2011; Accepted 26 July 2011

1. Introduction

The unusual meteorological conditions in the polar regions result from unique solar cycles combined with high surface albedo and long wave emissivity. The limited geographical extent of these conditions does not imply a lack of interaction with the rest of the Earth, however. Drivers from lower latitudes such as anthropogenic aerosols (Quinn *et al.*, 2007) and climate forcings (Gillett *et al.*, 2008) and natural atmospheric variability (Moritz *et al.*, 2002) can also have a significant impact on the polar climate. The converse is also true, for example the Arctic sea ice, an indicator of local climate (Curry *et al.*, 1995), impacts Northern Hemisphere weather patterns (Francis *et al.*, 2009) and, more generally, global circulation (Budikova, 2009). Polar atmospheric conditions, and the difficulties that models have in accurately representing them (Randall *et al.*, 1998), thus present measurement opportunities of both local and global significance. However, these same conditions often also present the greatest challenges to taking such measurements.

The primary historical and contemporary means of profiling the atmosphere has been the radiosonde. These have been used for the past 50 years at many polar locations and so provide long term data records (Lesins *et al.*, 2010, for example). However, profiles of vastly improved temporal and vertical resolution of atmospheric optical properties, plus derived physical properties, can be obtained by using a light detection and ranging

instrument or lidar. In this paper lidar measurements from within the Arctic and Antarctic circles ($66^{\circ}33'$ parallels), concentrating on the troposphere, are reviewed. There has been substantial work done in the middle atmosphere, however this is beyond the scope of this paper and shall only be noted when there is overlap with tropospheric measurements. The goal of this review is not only to highlight the work done in some of the world's most isolated locations, but also to place these measurements in the context of current understanding of polar atmospheric processes.

As way of introduction, Section 2 has a brief description of the technical and mathematical basis of the lidar techniques used. Definitions for different forms of nomenclature are given for those unfamiliar with the field. Operating in the polar regions places considerable limitations on the scope of measurements that can be made compared to a mid-latitude site. Section 3 briefly addresses some of the technical challenges faced. Following this is a catalogue of tropospheric lidar installations in the Antarctic and Arctic, Section 4, along with the major results recorded at these locations. The Arctic, in particular, has seen concentrated aircraft- and ship-based measurement campaigns and Section 5 details those using lidars from 1986 through to the present. With global coverage, lidars on polar-orbiting satellites have radically changed the measurement possibilities over the poles, traditionally regions with a paucity of measurements, and two such satellites are presented in Section 6. Paralleling the techniques discussed in Section 2, some of the most significant findings derived from aerosol, cloud, water vapour and ozone measurements are discussed in

* Correspondence to: G. J. Nott, Department of Physics and Atmospheric Science, 1459 Oxford Street, Dalhousie University, Halifax, Nova Scotia B3H 4R2, Canada. E-mail: graeme.nott@dal.ca

Section 7. Finally, discussion in Section 8 will centre on the future of lidars and their role in addressing some of the outstanding questions about the polar troposphere.

2. Introduction to lidar retrievals

It is not the purpose of this paper to describe lidar hardware, instrumentation, or analysis in depth, readers new to the field are referred to Weitkamp (2005) which is an excellent resource. However, retrieval techniques are discussed briefly as these elucidate atmospheric parameters that are mentioned in subsequent sections.

A lidar is a time-of-flight instrument where the signal scattered back into the receiver is a function of time, and thus distance from the transmitter. For atmospheric instruments where the lidar is directed upwards, this is given as altitude. For the simplest case of a single wavelength elastic backscatter lidar the power received in each time (and thus altitude) bin, $P(\lambda, z)$, is:

$$P(\lambda, z) = P_0(\lambda)\eta(\lambda)O(z)\Delta z \frac{A}{z^2}\beta_\pi(\lambda, z) \times \exp\left\{-2\int_0^z \alpha(\lambda, z') dz'\right\}. \quad (1)$$

P_0 is the transmitted power, η is the system efficiency at the wavelength of interest, λ , and $O(z)$ is the overlap function which describes the fraction of the laser beam that is within the field of view of the receiver telescope. The z dependence of the overlap function is different for each particular lidar and falls from one at high altitudes to zero at altitudes approaching ground level. The solid angle subtended by the telescope of area A , is given by A/z^2 . The backscatter coefficient, $\beta_\pi(\lambda, z)$, is the product of the concentration of scatterers in the sampled volume and their differential backscatter cross-section. The π will be dropped for clarity and indeed it should be noted that for bistatic lidars the scattering cross-section at an angle other than π is possible (Olofson *et al.*, 2009 for example). The exponential term is the two-way fractional transmission of light through an atmosphere with an extinction coefficient α .

2.1. Aerosol and cloud retrieval

The major issue with the retrieval from an elastic backscatter lidar, that is one with a single transmitted and received wavelength, is that Equation (1) is under defined with two unknown atmospheric properties, the extinction and backscatter coefficients. α and β are related through the lidar ratio, $S(z) = \alpha(z)/\beta(z)$, and if the aerosol being measured is known and well characterized then S may be known and so α and β found. However, this is often not possible in the polar regions which means that α and β cannot be determined (see Ansmann and Müller, 2005 and references therein for details). The backscatter and extinction coefficients are the sum of both molecular and aerosol contributions, where ‘aerosol’ in this case is used

to denote any non-gaseous scatterer such as dust, cloud droplets, or ice crystals. As the molecular coefficients can be calculated from scattering theory, their ratio is $8\pi/3$ sr, when not mentioned explicitly the lidar ratio is assumed to be that for aerosols only.

In cases where α and β cannot be determined, the parameter commonly given is the backscatter ratio, also called the Rayleigh ratio in early papers, which is the ratio of total backscatter coefficient (aerosol plus molecular) to the molecular backscatter coefficient, $R(z) = \{\beta_{\text{aer}}(z) + \beta_{\text{mol}}(z)\}/\beta_{\text{mol}}(z)$. The molecular contribution, $\beta_{\text{mol}}(z)$, is calculated using a standard atmosphere or radiosonde profiles. In clear air the backscatter ratio is unity and increases in the presence of aerosols and clouds. It is sometimes presented as $1/R(z)$ (Pitts *et al.*, 2009) or $1 - 1/R(z)$ (Adachi *et al.*, 2001) so that values are between zero and one.

Instead of relying on a simulated molecular lidar return, the lidar ratio may be obtained with a more complex lidar technique, one that separately measures the backscattered signal solely from molecules. In this way the contribution purely from the aerosol component can be derived. Two instruments capable of this are the Raman lidar and the high spectral resolution lidar (HSRL). The Raman lidar uses a channel centred on the wavelength of a vibrational Raman line of nitrogen or sometimes oxygen (Ansmann *et al.*, 1992). The change in wavelength from that of the laser is dependent on the chosen molecular species and the strength of the return signal is dependent on the density of that molecule. The Raman signal is several orders of magnitude weaker than the elastic signal so that a high power-aperture lidar and spectrally-narrow filters are required for daytime measurements. The HSRL separates the molecular signal based on the large Doppler broadening of molecules compared to the much heavier aerosols (Shiple *et al.*, 1983). The elastic backscattering provides a large signal but the technique requires precise control of both the transmitter and receiver spectral characteristics. The aerosol extinction coefficient, α_{aer} , profile can be derived from the pure molecular backscattered signal and the aerosol backscatter coefficient, β_{aer} , can be obtained by taking the ratio of the molecular and total return signals. Thus, with either of the Raman or HSRL techniques the lidar ratio can be measured directly.

Some points to note about nomenclature. Backscatter coefficient may also be called the volume backscatter cross-section, having units of $\text{m}^{-1} \text{sr}^{-1}$. The prefix ‘attenuated’ is added to identify explicitly when the aerosol differential extinction has not been accounted for. If ‘total’ (or sometimes ‘pseudo’) is prefixed, this means that the quantity includes the molecular contribution as well as that from aerosols.

The colour ratio, χ or sometimes just CR , describes the change in backscatter coefficient with wavelength in a similar manner to the Ångström exponent that describes the wavelength dependence of the extinction coefficient. $\chi(z) = \beta(\lambda_{\text{longer}}, z)/\beta(\lambda_{\text{shorter}}, z)$ so that at visible wavelengths $\chi(z)$ varies from close to zero for molecules

to around one for large cloud particles (Tao *et al.*, 2008). The colour ratio is also sometimes defined in terms of the backscatter ratio, $\chi'(z) = \{R(\lambda_{\text{longer},z}) - 1\} / \{R(\lambda_{\text{shorter},z}) - 1\}$ (Liu and Mishchenko, 2001) which varies from one for a molecular return to approximately $\lambda_{\text{longer}}^4 / \lambda_{\text{shorter}}^4$ for large particles.

Another microphysical property of importance is particle shape which, for hydrometeors, is dependent on the phase state. A depolarization lidar (see Sassen, 2005 for an introduction) separately measures light parallel and perpendicular to the plane of the transmitted light. These two return signals allow the total depolarization ratio, δ , to be calculated as the ratio of perpendicular to parallel backscatter coefficients, $\delta(z) = \beta_{\perp}(z) / \beta_{\parallel}(z)$. As a rule δ is zero for water droplets, ~ 0.03 for air (Bodhaine *et al.*, 1999), and ~ 0.25 – 0.6 for ideal ice crystals ranging from thin plates to long columns (Noel *et al.*, 2004; Sassen, 2005). If the backscatter coefficients include the molecular component then the total depolarization ratio is calculated. Note that less frequently the depolarization ratio may also be defined as $\delta'(z) = \beta_{\perp}(z) / \{\beta_{\parallel}(z) + \beta_{\perp}(z)\}$. When referencing works that use this definition, $\delta'(z)$ has been converted to $\delta(z)$ for consistency. Either linear or circular depolarization ratio may be measured depending on the optical layout of the lidar. For random particles in a small sampling volume, one can be calculated from the other (Mishchenko and Hovenier, 1995).

2.2. Water vapour retrieval

Water vapour has been shown to be a significant contributor to Arctic amplification, being a strong feedback mechanism for regional atmospheric change (Soden and Held, 2006). Unlike column measurements, from microwave radiometers for example, lidars provide the vertical distribution of the water vapour which is important for understanding the associated feedback processes (Bony *et al.*, 2006). The water vapour mixing ratio can be determined by measuring the Raman backscatter of water vapour and of nitrogen, where nitrogen is a proxy for dry air. For an absolute mass mixing ratio one must carefully calculate the spectral response of the instrument (Vaughan *et al.*, 1988), calibrate the integrated profile with a column water vapour measurement (Turner and Goldsmith, 1999), or calibrate with an *in situ* measurement such as that from a radiosonde (Ferrare *et al.*, 1995).

2.3. Temperature retrieval

The Rayleigh lidar technique (Hauchecorne and Chanan, 1980), commonly used for middle atmosphere temperature retrieval, cannot be used in the troposphere due to aerosol interference, so a technique that obtains the temperature from the molecular return is required. Behrendt (2005) reviews different lidar temperature measurements and the one of interest here is the rotational Raman technique. The backscatter cross-section of the pure rotational Raman lines of nitrogen and oxygen (the lines of these species overlap) has a Maxwell–Boltzmann distribution

and so depends on the atmospheric temperature. With two measurement channels at wavelengths covering different regions of the distribution, a differential measurement of temperature can be made (Cooney, 1972). Being a difference measurement, the technique is insensitive to the presence of aerosols and thin clouds. A proportionality factor to relate the ratio of the channels to atmospheric temperature can be determined by calibration with a radiosonde profile.

2.4. Ozone retrieval

Ozone profiles can be obtained with an ultraviolet differential absorption lidar (DIAL). A DIAL is an elastic backscatter lidar with two or more channels, the wavelengths of which are chosen for high and low absorption cross-sections of the species of interest. DIAL measurements of stratospheric ozone have been undertaken for some time in the polar regions. The spring time southern hemisphere ozone hole and northern hemisphere depletion, the role of polar stratospheric clouds in ozone destruction, the influence of the polar vortex, and other research interests have all driven middle atmosphere lidar observations in the Arctic (Donovan *et al.*, 1995) and Antarctic (Santacesaria *et al.*, 1999). The DIAL technique is equally useful for tropospheric ozone profiles, although the wavelengths used need to be optimized for the altitude range of interest.

3. Technical challenges

Although lidars were implemented soon after the invention of the laser (see Fiocco and Smullin, 1963 for example) and the technology and techniques are universal, implementing this technology in the polar regions remains a significant challenge. The challenges are environmental: power, temperature control, clear and consistent access to the sky, and logistical: access, telecommunications, and the cost thereof. The required investment has resulted in comparatively fewer lidars in the polar regions and their measurement capabilities, being constrained by instrument complexity, has generally lagged those of mid-latitude lidars. A class of lidars that is popular for installation in more inhospitable locales are based on micropulse lasers. These systems are eye-safe and usually autonomous and the Micro Pulse Lidar Network (MPLNET) includes lidars in both the Arctic and Antarctic. The high repetition rate of the micropulse laser ensures good counting statistics, however the low energy *per* pulse means that weak signals, either due to a small scattering cross-section or significant solar influence, are difficult to measure. Micropulse lidars are generally confined to elastic backscatter measurements.

Micropulse lidars can be positioned to operate out of a standard window (Shiobara *et al.*, 2003), however more complicated systems tend to be set up in a customized building where particular requirements of the instrument can be more easily met. Generally, an open hatch or

optical-quality window in the roof is required, such windows need to be kept free of snow on the outside and condensation on the inside. If an open hatch is used the ambient telescope may be separated from the temperature-controlled room containing the laser and receiver. High-powered lasers produce a large amount of heat and the regularization of laboratory temperature is important for narrow linewidth lasers and optical filters. This includes spatially: floors tend to be very cold while ceilings are hot, and seasonally, with 24 h sunlight and thick insulation, cooling in the summer can be more difficult than winter-time heating. Temperature issues are even more troublesome for aircraft-mounted lidars. Hanger facilities are minimal or non-existent so electrical heating of the lidar enclosure may be required to ensure optics and laser crystals are not subjected to very low ambient temperatures.

Three main modes of operation have developed. Systems that require an on-site operator generally operate in a short and intensive campaign mode with a skilled operator who is able to maintain as well as operate the lidar. If satellite bandwidth is adequate, systems can be operated remotely or autonomously saving the expense of having a local operator. Although more measurements can be collected this way, significant downtime can result from a hardware failure. An intermediate mode is where the lidar is essentially 'plug-and-play' but requires a local operator to start and stop data acquisition, assess local operating conditions, and shut down in cases of adverse weather conditions, overflying aircraft and the like.

Atmospheric conditions in the polar regions also contribute to the difficulty in lidar measurements. Although the aerosol loading in the Arctic may be comparable to that of mid-latitudes, Arctic haze aerosol optical depths peak at 0.12–0.25 at $\lambda = 500$ nm, the air is very much cleaner in the Antarctic with median aerosol optical depths (500 nm) ranging from 0.06 on the coast to 0.015 on the plateau (Tomasi *et al.*, 2007). Water vapour content is also very low once the sea ice forms in the winter. Background levels of precipitable water hover around 1–2 mm (Doyle *et al.*, 2011) while the global average is 25 mm (Randel *et al.*, 1996). These low levels require either a system with greater sensitivity or longer integration times than for a similar mid-latitude measurement.

4. Lidar installations

Here past and present tropospheric lidar installations in both the Arctic and Antarctic are catalogued. A somewhat arbitrary distinction has been made between fixed-location installations and the campaigns described in Section 5. Lidars are described for each installation along with some interesting measurements taken at these locations. Figure 1 shows the installations referred to in the text.

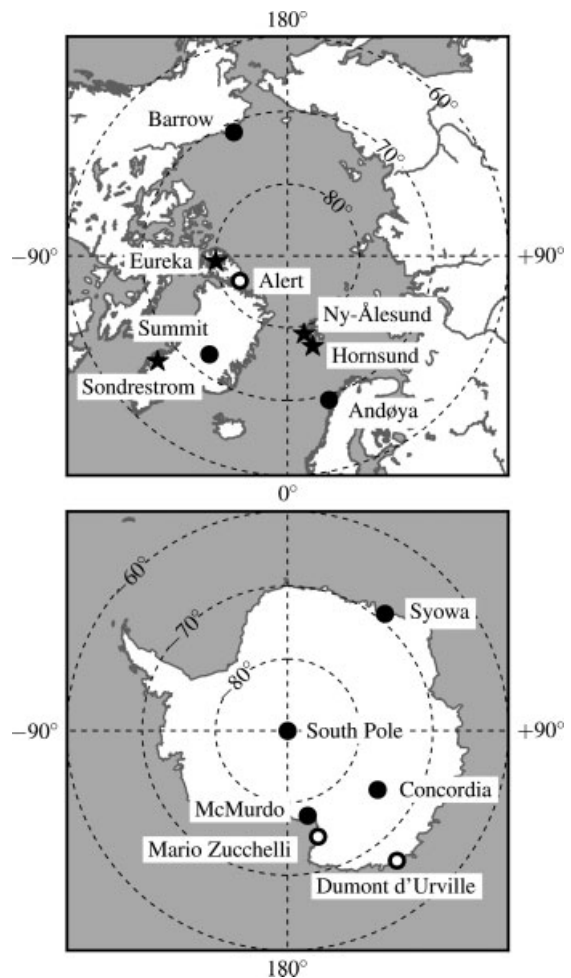


Figure 1. Arctic and Antarctic tropospheric lidar installations discussed in the text. Circles represent aerosol lidars while stars indicate locations with additional lidar capabilities. Closed symbols represent lidars that are currently operational while open symbols are no longer operational.

4.1. The Antarctic

4.1.1. South pole

The first lidar in Antarctica was installed in the 1974/1975 austral summer at the Amundsen-Scott South Pole station (Smiley *et al.*, 1975). Backscatter data were collected for 2 years before the system was upgraded to measure depolarization during the 1976/1977 summer (Smiley and Morley, 1981). Perhaps the most important observation reported was that diamond dust, suspended ice crystals in a clear sky, was capped by a sub-visible cloud 75% of the time. This was subsequently seen a decade later in the Arctic (Intrieri and Shupe, 2004) and is discussed further in Section 7.1.2. This system was relocated briefly to Palmer Station ($64^{\circ}46'S$, $64^{\circ}03'W$) although no results from this location have been found (Smiley *et al.*, 1979). A micropulse system was installed in 1999 and is still operating as part of MPLNET. Measurements have been used to create tropospheric cloud climatologies (Mahesh *et al.*, 2005) and characterize blowing snow events (Mahesh *et al.*, 2003). Blowing snow has an average vertical extent of 400 m with 50% of the layers being less than 200 m thick. A climatology of surface

observations reveals a slight increase in occurrence probability of blowing snow events between 1992 and 2001, with the winter having a considerably higher occurrence of blowing snow compared to the summer. This is reflected in the ice particle habit characterization of Lawson *et al.* (2006) and Walden *et al.* (2003) that is discussed in Section 7.2.2.

4.1.2. Syowa

Iwasaka (1985) present the first lidar measurements of polar stratospheric clouds from Syowa (69°00'S 39°35'E) in 1983, after they had recently been observed in satellite measurements (McCormick *et al.*, 1982). Since that time most of the work at Syowa has concentrated on the stratosphere and mesosphere. A commercial micropulse system was installed in 2001 as part of MPLNET and has been used to produce climatologies of tropospheric clouds (Shiobara *et al.*, 2003).

4.1.3. Mario Zucchelli

A depolarization aerosol lidar was operated at the Italian base at Terra Nova Bay on the Ross Sea (74°42'S 164°07'E) for several years. A review of the instrument and cloud statistics from the 1987/1988 summer is given by Sacco *et al.* (1989) although apparently it was operated for at least 3 years based on a comment by Stefanutti *et al.* (1992a). Clear sky dominated during the January–February measurement period with clouds between the ground and 2 km and 2–4 km both having an occurrence frequency of 15%. Liquid water droplets were frequently observed in the low clouds.

4.1.4. Dumont d'Urville

After the installation of a depolarization lidar at Dumont d'Urville (66°40'S 140°01'E) in 1989, Del Guasta *et al.* (1993) present a cloud climatology based on continuous measurements from 1 year. Cloud heights have a skewed distribution with low clouds most common. As this was an elastic system, a simulated molecular return was calculated from radiosonde profiles. Calculation of lidar ratio was complicated by multiple scattering, however for optically thin ice clouds the median lidar ratio was around 29 and showed almost no trend with mid-cloud temperature between 200 and 240 K (adapted from Del Guasta *et al.*, 1993, figure 19a). For temperatures above 240 K, the lidar ratio decreased. Total depolarization ratio measurements of cirrus show no overt trend over temperatures 193–233 K, the median being 0.37 (Del Guasta and Vallar, 2003a, 2003b).

In the 1990/1991 summer, the existing 532 nm depolarization lidar was expanded with ultraviolet aerosol and tropospheric and stratospheric ozone channels (Stefanutti *et al.*, 1992b). The ozone channel wavelengths were separately optimized for two altitude regions, 2–12 and 12–40 km although this system was primarily used for stratospheric cloud and aerosol research (Santacesaria *et al.*, 2001). The lidar was replaced in 2006 with a new

stratospheric system as part of the Network for the Detection of Atmospheric Composition Change (NDACC) and there is no longer a tropospheric lidar at Dumont d'Urville.

4.1.5. McMurdo

The lidars located at McMurdo (77°51'S 166°40'E) from 1990 through to the present have been primarily designed and used for measurements of polar stratospheric clouds (Adriani *et al.*, 2004 for example), stratospheric temperatures, and volcanic aerosols (Di Donfrancesco *et al.*, 2000). The current lidar is an NDACC instrument for measuring stratospheric aerosols and temperature and tropospheric elastic and nitrogen Raman profiles.

4.1.6. Concordia

The French–Italian station at Dome C (75°06'S 123°20'E) was equipped with a depolarization lidar in 2007. Preliminary observations of blowing snow, mixed-phase clouds, and cirrus clouds are presented by Castagnoli and Vitale (2010). Perhaps most interestingly, a pollution plume from the station generators is also shown, it was identified by wind direction and associated with high backscatter and low depolarization ratios.

4.2. The Arctic

4.2.1. Alert

Environment Canada operates a small atmospheric and meteorological facility at Alert (82°30'N, 62°20'W). An elastic lidar was operated there from 1984 until 1986 and was used to complement both surface aerosol measurements and aircraft campaigns in the area (Hoff, 1988).

4.2.2. Ny-Ålesund

An atmospheric observatory at Ny-Ålesund (78°55'N 11°56'E) was commissioned in 1995 and houses a stratospheric lidar (in operation since 1988), the Koldewey-Aerosol-Raman-Lidar (KARL) since 1999, and an automated micropulse lidar since 2003 that is part of MPLNET and NDACC. KARL includes aerosol channels, depolarization, and ultraviolet and visible water vapour Raman channels. In 2008 the lidar was significantly rebuilt with enhanced multi-wavelength aerosol measurements and 0.45–30 km altitude range (Hoffmann *et al.*, 2010). Hoffmann *et al.* (2009) present cloud and aerosol measurements made in March and April 2007 and characterize air masses as a function of depolarization and backscatter ratios, although the time span of this study (145 h) perhaps precludes general conclusions. With the Raman lidar, the lidar ratio was found for both ice and mixed-phase clouds (see Table I) and two weak aerosol episodes. Haze lidar ratios of 80 ± 12 and 60 ± 10 sr were found in the visible and ultraviolet respectively while an elevated aerosol event had lidar ratios of 64.3 and 39.6 sr.

Table I. Lidar ratio, S , of polar clouds.

S (sr)	Instrument	Cloud description	Ref.
14.5	Nephelometer	Drizzle	Gayet <i>et al.</i> (2007)
13.8	Nephelometer	Ice cloud	Gayet <i>et al.</i> (2007)
27 ± 7	Nephelometer	Subvisible ice cloud	Lampert <i>et al.</i> (2009)
21 ± 6	Combined ^a	Subvisible ice cloud	Lampert <i>et al.</i> (2009)
19.8	532/607 lidar	Ice clouds, 4.5 km	Lampert <i>et al.</i> (2010)
17.9	355/387 lidar	Ice clouds, 4.5 km	Lampert <i>et al.</i> (2010)
14.4	532/607 lidar	Mixed-phase cloud, 3–3.5 km	Lampert <i>et al.</i> (2010)
6.5	355/387 lidar	Mixed-phase cloud, 3–3.5 km	Lampert <i>et al.</i> (2010)
37.0 ± 1.0	532/607 lidar	Lidar ice clouds, 2.6 km	Lampert <i>et al.</i> (2010)
3.0 ± 0.2	355/387 lidar	Lidar ice clouds, 2.6 km	Lampert <i>et al.</i> (2010)
10	532/607 lidar	Ice and/or sea salt, 1 km	Gerding <i>et al.</i> (2004)
10	532/607 lidar	Ice cloud, 10.4–10.8 km	Hoffmann <i>et al.</i> (2009)
18	532/607 lidar	Mixed-phase cloud, 2.2–3.4 km	Hoffmann <i>et al.</i> (2009)
25 ± 12	532/607 lidar	Ice cloud, 6–8 km	Nott <i>et al.</i> (2011)
20 ± 9	355/387 lidar	Ice cloud, 6–8 km	Nott <i>et al.</i> (2011)

^a Average of nephelometer, lidar, and combined lidar and albedometer techniques.

4.2.3. Eureka

From 1993 until 1997 winter-time aerosol measurements were made at Eureka (79°59'N, 85°56'W) with an elastic lidar. Backscatter ratio and depolarization profiles, combined with meteorological data, were used to quantify clouds and Arctic haze and the conditions under which they form (Ishii *et al.*, 1999). Haze events, frequently below 3 km and occasionally at 3–5 km, were generally found to occur at humidities less than 60% over ice, while clouds dominate at >80% over ice. Figure 2 shows the peak backscatter and depolarization ratios as a function of relative humidity from this study, the aerosols having significantly smaller depolarization.

As part of the Study of Environmental Arctic Change programme (SEARCH) an HSRL has been operating nearly continuously from 2005 to 2010, measuring backscatter and depolarization ratio from 70 m up to approximately 15 km (Eloranta *et al.*, 2006). Statistical studies of such long-term, continuous measurements are valuable for identifying scatterer type based on their behaviour without limiting the applicability of the conclusions to a particular season or year. Using both the HSRL and a co-located millimetre cloud radar, Bourdages *et al.* (2009) classified particle populations based on the backscatter at two very different wavelengths (532 and 8.6 mm) and the 532 nm depolarization ratio. The regions of depolarization ratio/colour ratio space are divided up based on the observed species in individual profiles to create the classifications shown in Figure 3. The colour ratio is used to infer size information. Since 2008 a tropospheric ozone-DIAL and Raman lidar, operating under the auspices of the Canadian Network for the Detection of Atmospheric Change (CANDAC), have been co-located with the HSRL. The CANDAC Rayleigh-Mie-Raman lidar has aerosol channels in the visible and ultraviolet as well as water vapour and rotational Raman temperature channels. To the author's knowledge the first tropospheric temperature lidar profile measured in the polar regions

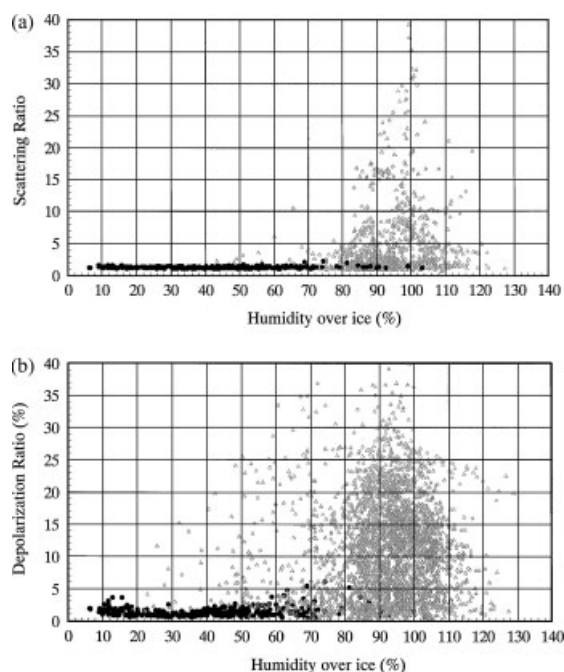


Figure 2. Relationship between scattering ratio, R (a), and depolarization ratio, δ' (b), and relative humidity over ice for clouds, Δ , and haze, \bullet , particles. Data from winters 1993–1997 at Eureka (from Ishii *et al.*, 1999 with permission from Elsevier).

has been made with this system although at time of writing a more complete analysis is not available (Nott *et al.*, 2011).

4.2.4. Sondrestrom

Since 1993 a middle atmosphere lidar has operated as part of the Arctic Lidar Technology (ARCLITE) facility at Sondrestrom, Greenland (67°00'N, 50°55'W) (Thayer *et al.*, 1997). Raman nitrogen and water vapour channels at 607 and 660 nm have subsequently been added with first water vapour measurements over 1–10 km being presented by Neely and Thayer (2010).

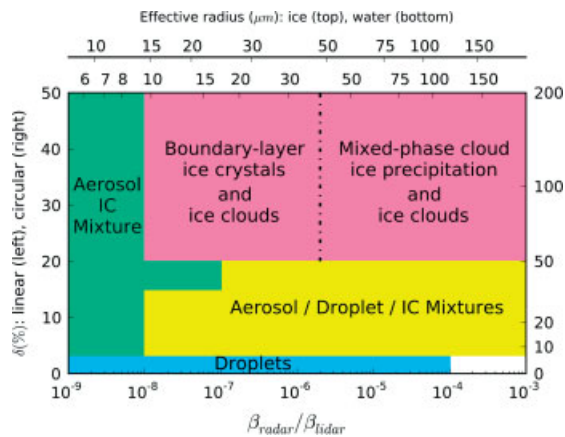


Figure 3. Classification of wintertime atmospheric particles and their mixtures from Eureka, 2005–2008. Effective radii for liquid droplets and spherical ice crystals (IC) are calculated for a given colour ratio, although this is only valid where there are no aerosols (from Bourdages *et al.*, 2009).

4.2.5. Barrow

The North Slope of Alaska site is part of the Atmospheric Radiation Measurement (ARM) programme near Barrow, Alaska (71°19'N, 156°37'W). Currently there is a micropulse lidar installed on site. The long-term nature of the ARM site has enabled a 10 year cloud climatology to be assembled, 5 years of which were using a lidar and radar (a ceilometer was also used over the period 1998–2008). Average seasonal cloud occurrences are 65% (winter), 68% (spring), 83% (summer), and 89% (autumn) with an annual mean change of -4.8% per year seen over the 10 year period (Dong *et al.*, 2010).

4.2.6. Andøya

The Arctic Lidar Observatory for Middle Atmospheric Research (ALOMAR), is part of the Andøya Rocket Range facility (69°16'N, 16°00'E) and primarily measures middle atmosphere temperature, ozone, and wind speeds (von Zahn *et al.*, 2000). A dedicated tropospheric lidar was added in 2005 to extend measurements down from the tropopause (Frioud *et al.*, 2006). In 2006 a polarization-sensitive bistatic lidar receiver was used to study the ice crystals in cirrus clouds. The bistatic arrangement allowed measurements of scattering angles 130–170° along with the backscatter as collected by the regular detection system (Olofson *et al.*, 2009).

4.2.7. Hornsund

A tropospheric lidar was installed at the Polish research station at Hornsund, Svalbard (77°00'N 15°33'E) in 2009. There are elastic measurements at 1064, 532, and 355 nm as well as nitrogen and water vapour Raman channels in the ultraviolet (Pietruczuk and Karasiński, 2010).

4.2.8. Summit

As part of the 4 year Integrated Characterization of Energy, Clouds, Atmospheric State, and Precipitation at

Summit (ICECAPS) campaign, a depolarization lidar was installed at Summit, Greenland (72°36'N 38°25'W) in 2010. This system measures the return signal in three planes of polarization: parallel, perpendicular and 45° (Neely *et al.*, 2010). Additionally a micropulse lidar is on site as part of this measurement campaign. In contrast to the other facilities in the Arctic, Summit is significantly above sea level at an altitude of 3.2 km. Measurements will be less influenced by regional changes and so provide large-scale observations and an interesting counterpoint to those from sea level instruments.

5. Campaigns

While an effort has been made to summarize the achievements of those campaigns in which tropospheric lidars played a significant role, the authors cannot claim a complete listing of all relevant campaigns. All but one campaign are from the Arctic, the greater logistical challenges of the Antarctic mean that even short-term programmes tend to be based out of permanent research stations.

5.1. Antarctic ferry flight measurements

The single aircraft campaign in the Antarctic was in the summer of 1986 (Morley *et al.*, 1989). A nadir-pointing 532 nm elastic lidar was flown on ferry flights between McMurdo, the South Pole station, and Siple (75°55'S 83°55'W) to look at cloud cover over Western Antarctica. Stable layers at 2.5–3 km were predominant over the Ross ice shelf, these were judged to be mixed-phase or liquid clouds due to the total extinction of the beam. Deep cirrus clouds, frequently displaying virga, were common over the ice cap.

5.2. Arctic gas and aerosol sampling program

These campaigns were held in 1983, 1986, 1989 and 1992 across the western Arctic between Norway and Alaska. The second Arctic Gas and Aerosol Sampling Program (AGASP-II) in 1986 used an aircraft-mounted nadir-looking near infrared elastic backscatter lidar and *in situ* instruments to investigate the role of haze in the spring-time Arctic (Morley *et al.*, 1990). Brock *et al.* (1990) report multiple thin haze layers of thickness between 30 and 60 m with horizontal extents from as small as 20 km. Thicker, well-mixed layers with vertical thicknesses around 500 m were found to extend for 500 km. Sulphates dominated the haze layers with loading within the haze similarly horizontally and vertically inhomogeneous. Fine mode sulphur concentrations were calculated to peak at $3 \mu\text{g m}^{-3}$. Thin layers were advected into the Arctic by narrow jets from further south while the thermal stability of the polar air mass maintained the striated nature of the haze (Radke *et al.*, 1989).

Schnell *et al.* (1989) used the same lidar to investigate plumes of hydrometers injected into the atmosphere

over leads in the sea-ice. Leads of widths 10 km or greater generated plumes energetic enough to escape the boundary layer temperature inversion and were observed up to altitudes of 4 km.

5.3. Canadian Arctic Haze Study

The Canadian Arctic Haze Study was held at Alert coincident with AGASP-II, and compared ground-based ruby lidar profiles to *in situ* measurements (Leaich *et al.*, 1987). They report that fine particles dominated coarse mode with particles predominantly in hydrated form with reasonably uniform depolarization ratios that were less than 0.18 and usually around 0.08. These numbers are converted from δ' to δ (Hoff, 1988) and also possibly include an instrumental component of ~ 0.05 , although this is unclear.

5.4. Arctic Boundary Layer Expedition

The Arctic Boundary Layer Expedition (ABLE 3A) was conducted in July–August 1988 and covered Greenland, Northern Canada and Alaska. The primary focus was on atmosphere–biosphere interaction and measurements of relevant chemical species (Harriss *et al.*, 1992). An airborne DIAL was used to measure ozone concentrations from the ground to the tropopause and is interesting in that the transmitted light was split into zenith- and nadir-pointing components to measure above and below the flight deck simultaneously. *In situ* ozone measurements were used to constrain the retrieval within the overlap regions (Browell *et al.*, 1992). Results from these measurements are discussed in Section 7.4.

5.5. Arctic Haze

The Arctic Haze campaign of 1993/1994 (Arctic Haze, 1997) made use of an aircraft-mounted nadir-looking elastic lidar. Haze/aerosol layers measured over Siberia and the Siberian-Arctic were concentrated in the lowest 2 km. Backscatter increased by an order of magnitude from 80°N to regions closer to polluted areas. Total depolarization ratios were 0.01–0.15 with the higher values being found close to the aerosol source regions. Horizontal scattering profiles confirmed prior reports of the spatial inhomogeneity of the haze layers with scattering coefficients varying over ranges of several to tens of kilometres (Khattatov *et al.*, 1997).

5.6. Surface Heat Budget of the Arctic Ocean

The Surface Heat Budget of the Arctic Ocean (SHEBA) research programme (Uttal *et al.*, 2002), a multi-disciplinary effort to measure the state and processes of the Arctic ocean, sea-ice, and atmosphere over an entire year, has yielded a wealth of information about the radiative processes of the Arctic. Measurements were taken on a drifting icebreaker from October 1997 to October 1998 with the lidar being a 532 nm elastic backscatter and

depolarization-sensitive lidar oriented at 5° off-zenith. Cloud statistics were obtained by combining the lidar and cloud radar datasets (Intrieri *et al.*, 2002a): for a comparison of cloud statistics gleaned from different instruments and observations, including the lidar/radar see Wyser and Jones (2005). Cloud base heights were dominated by those in the 0–1 km range. Liquid and solid phase returns were demarcated at a depolarization ratio of 0.11 and liquid water in clouds was detected all year round with occurrence probabilities of 95% over summer and 45% during the winter. Mixed-phase clouds were concentrated in the lowest kilometre but were frequently observed up to 4.5 km and occasionally up to 6.5 km. Ice clouds occurred at all altitudes 0–10 km.

Using cloud boundaries from Intrieri *et al.* (2002a), radiosonde temperature profiles, and downwelling atmospheric radiance spectra as inputs, Turner (2005) calculated particle size and phase information for single-layer clouds between November and May. Mixed-phase and liquid clouds were found down to 240 K with the ice fraction displaying no appreciable trend with temperature as seen in Figure 4(c). Derived particle size distributions are presented with the mode radius in liquid clouds being 10 μm in the winter and 7 μm in the spring. However, significant questions remain about sizes in ice and mixed-phase clouds due to fact that crystal habit was unknown.

With cloud statistics and a radiative transfer model Intrieri *et al.* (2002b) calculated the cloud forcing on the surface throughout the year. Their data support earlier models (Curry and Ebert, 1992 for example) and observational data (Walsh and Chapman, 1998) and show a surface warming due to clouds during the entire year except for high summer when the strong short wave flux and reduced surface albedo result in a slight cooling. The 10 year climatology from Barrow also show this trend (Dong *et al.*, 2010). For mixed-phase clouds in May, Zuidema *et al.* (2005) report that for optical depths up to approximately 5 the radiative surface forcing is strongly dependent on the optical density, however for larger optical depths (and 60% of the mixed-phase clouds they studied over a 10 day period had an optical density greater than 6) the optical depth has minimal influence on the surface forcing as the short wave component dominates that of the long wave.

5.7. Arctic Clouds Experiment

Overlapping with SHEBA from April to July 1998, the First ISCCP (International Satellite Cloud Climatology Project) Regional Experiment-Arctic Clouds Experiment (FIRE.ACE) was a multiple aircraft campaign that concentrated on cloud and radiation measurements to improve polar satellite retrievals and models (Curry *et al.*, 2000). Two aircraft-mounted lidars were used. A lidar with 355 and 532 nm channels plus 1064 nm depolarization was mounted in an ER-2 flying at a nominal altitude of 18 km (McGill *et al.*, 2002). The second lidar was a simultaneous upward and downward-pointing 1064 nm

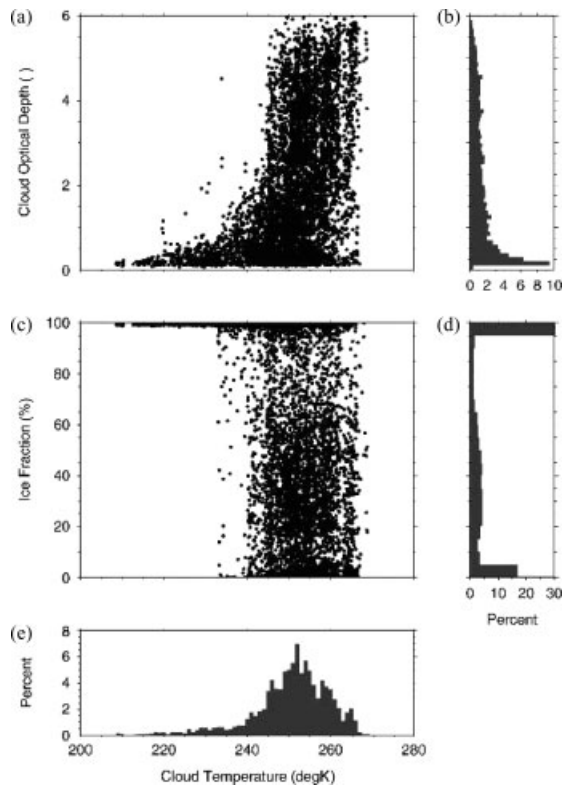


Figure 4. Optical depth and ice fraction of single layer clouds November 1997 to May 1998 at SHEBA. Optical depth scatter plot versus cloud temperature (a), and occurrence histogram (b). Ice fraction versus cloud temperature (c), and occurrence histogram (d). Frequency distribution of cloud temperatures (e) (from Turner, 2005).

depolarization lidar (described in Strawbridge and Snyder, 2001).

Lidar-derived boundary layer and cloud-top height over open water was observed to be two to four times that over unbroken sea ice (Gultepe *et al.*, 2003). Liquid water content and cloud particle sizes over open water were also larger with a higher proportion of irregular ice particles (60% compared to 40% over sea ice). The amount of open water, and the degree of melt on the sea ice as seen by Intrieri *et al.* (2002b), has a significant impact on radiative fluxes as well. Open water leads were measured to reduce the short wave upwelling radiation by 30–90% while long wave increased by 3–10% (Curry *et al.*, 2000, from Figure 9). The cloudiness or amount of sea smoke above the open water during these measurements was not mentioned and may, along with the amount of loose ice in the water, account for the range of influence on the irradiance.

Numerous measurements of ice crystal shapes were also made during this campaign. A number of authors have analysed the habit distributions and some care must be taken to note the different criteria that are used by each. Korolev *et al.* (1999) report that irregular ice particles dominate clouds from 273 to 228 K, however single crystals with evidence of melting/sublimation were classed as irregular. Rangno and Hobbs (2001) used six different types and their fragments for classification, irregulars now accounting for 37% with frozen drops

the next most prevalent at 20%. The fragmentation of these droplets, their riming, and collisions with fragile ice crystals result in mixed-phase clouds with ice concentrations in excess of ice nuclei concentrations in the cloud. They note that if using the same classification scheme as Korolev *et al.* (1999) they obtain comparable proportions of irregular to pristine crystals. In a cloud layer at 2.5–3 km (cloud top temperature, 258 K) where the SHEBA lidar indicated a liquid cloud top and ice and liquid mixed within the cloud layer, single particles were found to dominate with aggregates comprising <5% of all ice (Hobbs *et al.*, 2001). A second flight encountered 12 different cloud layers between 237 K (6.5 km) to 269 K (2.1 km) ranging from clouds of ice, through mixed-phase, to all liquid. Ice crystals observed were bullet rosettes, columns and plates, needles and sheaths, dendrites, stellars and graupel. This indicates the vertical and horizontal complexity of springtime clouds and the difficulty in comparing *in situ* measurements to fixed ground-based lidars. This particular aircraft was not fitted with a lidar.

5.8. Tropospheric Ozone Production about the Spring Equinox

The Tropospheric Ozone Production about the Spring Equinox (TOPSE, 2000) experiment used an aircraft-mounted ozone DIAL and *in situ* instruments for characterizing the chemical composition of the Arctic troposphere (Atlas *et al.*, 2003). The DIAL was the same upwards- and downwards-looking system that was used for ABLE-3A with an accuracy of better than 10% or 2 ppbv, whichever is greater (Browell *et al.*, 2003). Surface ozone depletions with horizontal extents of up to 600 km were seen and, although being observed as far south as over Hudson Bay (north from 59°N), all depletions originated over the Arctic Ocean (Ridley *et al.*, 2003). Average ozone increased between February and May and a correlation between concentration and aerosol backscatter ratio ($r^2 = 0.90$) was seen in the free troposphere, indicating that ozone was being transported into the Arctic over the spring (Browell *et al.*, 2003). However, concomitant measurements at Alert show that, at least when insolation was low, anthropogenic aerosols (measurements of black carbon, NO_y, and CO) are anticorrelated with surface-level ozone and so have a role to play in the depletion events (Bottenheim *et al.*, 2002). This is obviously not a simple matter as Ridley *et al.* (2003) found no consistent relationship between fine mode aerosol concentration and ozone depletions. That said, inspection of the ozone and aerosol data (Browell *et al.*, 2003, Figures 1, 2, and 4) indicate elevated backscatter ratios (>3) during ozone depletions within the boundary layer.

5.9. Arctic Study of Tropospheric Aerosol, Clouds and Radiation

The Arctic Study of Aerosol, Clouds and Radiation (ASTAR) programmes were a series of aircraft-based

measurements around Svalbard in spring 2000, 2004, and 2007 with complementary ground station measurements at Ny-Ålesund. Objectives centred around the characterization of springtime aerosols and this was extended to include clouds for 2004 and 2007 (Yamanouchi *et al.*, 2005). A downward-looking depolarization lidar (Stachlewska *et al.*, 2010) was flown as part of ASTAR 2004 (and 2007) and by combining the lidar returns with *in situ* size and phase measurements during a single flight, a lidar ratio was obtained for liquid and ice clouds of 14.5 and 13.8 sr respectively (Gayet *et al.*, 2007). However, extinction coefficients calculated with these values were significantly smaller than those measured *in situ* with the nephelometer. The authors cite the 80 min separation between the measurements as the most probable cause of this discrepancy.

During ASTAR 2007, an optically-thin ice cloud at 3 km was examined by Lampert *et al.* (2009) with the measured 532/355 nm colour ratio indicating particles with an effective diameter smaller than 5 μm . Particle backscatter coefficient varied between 0.3 and $5 \times 10^{-6} \text{ m}^{-1} \text{ sr}^{-1}$ throughout the cloud and *in situ* measurements confirmed the ethereal nature of the cloud with an average number concentration of only 0.5 l^{-1} and extinction of 0.01 km^{-1} . With a solar zenith angle of 70° , short wave downwelling was reduced by 3.2 W m^{-2} due to cloud reflection while long wave downwelling radiation increased beneath the cloud by 2.8 W m^{-2} , so the net cooling of -0.4 W m^{-2} is negligible on a local scale. As mentioned previously, however, during the winter the surface warming due to sub-visible clouds becomes more important. Fitting different ice crystal habits to the nephelometer-measured scattering phase function, a combination of spherical (1–100 μm) and 2:1 roughened hexagonal columns (20–900 μm) was found which gave a lidar ratio of 27 ± 7 sr. Using three independent methods, including that using the nephelometer, a mean lidar ratio of 21 ± 6 sr was determined.

Lampert *et al.* (2010) examines lidar measurements of different cloud and aerosol layers in spring 2007. The season was found to have typical cloud occurrence statistics but low Arctic haze levels. Hoffmann *et al.* (2009) notes that during this period the aerosol optical depth at $\lambda = 500 \text{ nm}$ was 0.05–0.08, compared to a 14 year average of 0.1. A layer of aerosol up to 2.5 km (241 K) was measured and was predominantly well-hydrated aerosols such as local sea-spray derived sulphates. A low level mixed-phase cloud at 700–1700 m with very high optical depth of 11–13 was measured with significant horizontal inhomogeneities, gaps in the cloud occurred on a kilometre scale. Cloud top was dominated by water with irregular ice crystals making up 22% at 252 K (1.7 km), 30% at 257 K (1 km), and 70% at 261 K (0.5 km) (Gayet *et al.*, 2009). Multiple layer ice and mixed-phase clouds were also investigated from 2.5 to 4.5 km. The uppermost layer displayed classic cirrus-like parameters,

aerosol backscatter of $3 \times 10^{-6} \text{ m}^{-1} \text{ sr}^{-1}$, peak depolarization of 0.7, lidar ratios of 19.8 (532 nm) and 17.9 sr (355 nm), and an optical depth of 0.11. The lower clouds displayed a significant variance in lidar ratio, indicating an unusual variety of crystal habits. Unfortunately, *in situ* crystal sampling was not carried out on this flight.

5.10. Mixed-Phase Arctic Cloud Experiment

Based over northern Alaska, the Mixed-phase Arctic Cloud Experiment (M-PACE) used *in situ* measurements, radiation, and lidar and radar measurements to study mixed-phase clouds in Autumn 2004. M-PACE was designed to facilitate improved modelling of mixed-phase clouds and a number of authors have presented modelled clouds based on these measurements (for example Klein *et al.*, 2009; Morrison *et al.*, 2009). Verlinde *et al.* (2007) presents a classical example of measurements of a precipitating, single-layer mixed-phase cloud with a depolarization ratio of approximately 0.05, a cloud base at 800 m and top height 1200–1300 m. The radar reflectivity, lidar backscatter and depolarization are shown in Figure 5. Snow was falling from the cloud with large irregular ice crystals dominating at the base of the cloud while frozen drizzle drops were detected at the cloud top. The vertical structure of the cloud radar reflectivity and the slight modulation in the cloud top height is due to the vertical motion within the cloud and its influence on the cloud microphysics. Shupe *et al.* (2008a) show that vertical air parcel motion varies considerably on a horizontal scale of approximately 5 km, vertical velocity was measured from 2.5 m s^{-1} upward to -1.5 m s^{-1} downward. A stronger updraft promotes greater ice fraction and larger particle sizes, resulting in a higher radar reflectivity.

5.11. Polar Study using Aircraft, Remote Sensing, Surface Measurements and Models, of Climate, Chemistry, Aerosols, and Transport (POLARCAT)

POLARCAT was an umbrella programme conducted as part of the 2007–2008 International Polar Year. Various campaigns were coordinated as part of POLARCAT: the Arctic Research of the Composition of the Troposphere from Aircraft and Satellites (ARCTAS, Jacob *et al.*, 2010), the Aerosol, Radiation, and Cloud Processes affecting Arctic Climate (ARCPAC, Brock *et al.*, 2011), the Greenland Aerosol and Chemistry Experiment (GRACE), International Chemistry Experiment in the Arctic Lower Troposphere (ICEALOT), plus others. Many of these campaigns used lidars in ways already described to augment radiation, chemical, or *in situ* measurements and results are in the process of being published.

Two evolving aerosol plumes from Asia and Europe were analysed by de Villiers *et al.* (2010) using backscatter ratio, depolarization and colour ratio from both

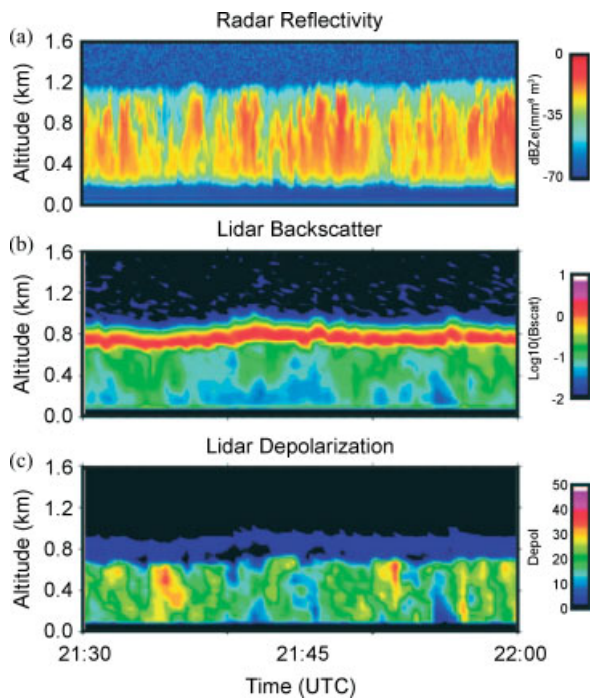


Figure 5. Cloud radar reflectivity (a), lidar backscatter (b), and lidar depolarization ratio (c) of a single layer mixed-phase cloud measured during M-PACE. Note that the lidar signal is fully attenuated before reaching the cloud top at 1.2 km (from Verlinde *et al.*, 2007).

satellite- and aircraft-mounted lidars. Despite the aerosol layers, measured between the ground and 4.5 km all being of similar optical depth, the particle characteristics were different. The aerosols originating in Europe were smaller (confirmed with *in situ* measurements) with a very low total depolarization ratio of 0.016 and low total colour ratio of 0.009. The Asian plume contained larger particles with slightly more depolarization, 0.021, and larger colour ratio, 0.13.

5.12. Pan-Arctic Measurements and Arctic Regional Climate Model Simulations (PAMARCMiP)

PAMARCMiP took place in April 2009 with a series of flights from Svalbard across the western Arctic to Barrow. The aircraft was fitted with two downward-looking lidars, a depolarization aerosol lidar (Stachlewska *et al.*, 2010) and a tropospheric ozone DIAL. Complementary ground-based measurements with the lidars at Ny-Ålesund, Eureka and Barrow were also taken. Over the entire region studied, the haze particles were found to be in the 130–200 nm size range with an Ångström exponent (412/675 nm) of 1.4–1.7, increasing from the surface to 4 km (Stone *et al.*, 2010). A second PAMARCMiP campaign was flown in spring 2011.

6. Satellite-based lidars

6.1. Geoscience Laser Altimeter System

Launched January 2003 on the Ice, Cloud and land Elevation Satellite (ICESat), the Geoscience Laser Altimeter

System (GLAS) was designed to measure the topography of the ice caps and profile aerosols and clouds. The instrument had two elastic backscatter channels, at 1064 and 532 nm and its polar orbit provided coverage between 86°S and 86°N. Spinhirne *et al.* (2005) found that cloud fraction was unevenly distributed over Antarctica in October 2003. Over the Southern Ocean and the Antarctic Peninsula the cloud fraction approached unity with Western Antarctica varying between 0.6 and 1. Low level stratus clouds dominated as has been seen in previous studies. Over Eastern Antarctica the skies are considerably clearer with the cloud fraction varying between 0 and 0.6. Ice clouds around the top of the troposphere become more prevalent as latitude increases. Unfortunately, all three lasers on board suffered from premature failure which resulted in reduced data volume and the decommissioning of ICESat from February 2010 (NASA, 2011).

6.2. Cloud-Aerosol Lidar with Orthogonal Polarization

The Cloud-Aerosol Lidar with Orthogonal Polarization (CALIOP) is mounted on the Cloud-Aerosol Lidar and Infrared Pathfinder Satellite Observations (CALIPSO) satellite and was launched in April 2006. It is part of the A-train constellation of satellites and has an orbit inclination of 98.2° (Winker *et al.*, 2009), thus providing coverage to 82° latitude. This wide-area coverage has proven immensely important in the polar regions where ground-based installations are few and far between. The lidar operates at 1064 and 532 nm with depolarization being measured at 532 nm. An overview of the lidar and analysis algorithms is given in the CALIPSO Special Collection (2009).

Given the volume of data gathered, statistical methods are being used to classify cloud particles and aerosols dependent on where a return falls in backscatter-depolarization space. Noel and Chepfer (2010) present measurements for different colour ratios, thus distinguishing between aerosols and clouds, comparing on-nadir (June 2006 to November 2007) and off-nadir (November 2007 to December 2008) CALIPSO data. Figure 6 shows the global frequency distribution of night time measurements as a function of integrated attenuated backscatter and depolarization ratios for $\chi > 0.7$. By limiting the figure data to large colour ratios, aerosol returns are excluded. The central region of increasing depolarization with backscatter is due to multiple scattering (Hu *et al.*, 2007 for example). Multiple scattering causes a gradual increase in depolarization ratio with cloud penetration depth and similar values to that expected from randomly oriented ice crystals are readily achievable due to the large, 90 m footprint of CALIOP (Yoshida *et al.*, 2010). Either side of the multiple scattering signature are the returns from ice crystals and this is discussed further in Section 7.2.2. Hu *et al.* (2009) show the same type of distribution as a function of temperature for both on- and off-nadir measurements and additionally use the correlation between backscatter and depolarization in adjacent

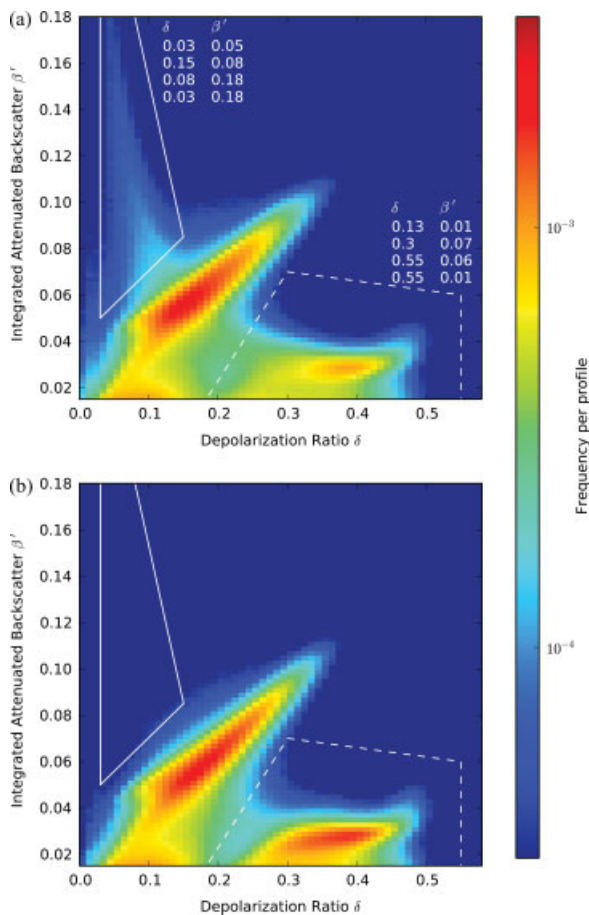


Figure 6. Integrated backscatter/depolarization ratio distributions of on-nadir (a), and off-nadir (b), global cloud returns from CALIPSO. The area outlined by the solid line indicates aligned ice while that outlined by the dashed line indicates randomly oriented ice. Coordinates of these regions are given in (a) (adapted from Noel and Chepfer, 2010).

footprints to help discriminate between horizontally oriented ice crystals and water clouds. At the time of writing there is some degradation of the depolarization data during the daytime, Sassen and Zhu (2009) note a change in depolarization ratio of approximately 0.11 between the day and night and this exceeds the physical diurnal variation of ice clouds seen by ground-based lidars.

Passive satellite measurements have significant problems discriminating between clouds and the snow- or ice-covered surface due to the boundary layer temperature inversion and low contrast in albedo. However, passive instruments do have significant spatial coverage, including all the way to the Poles, and long-term measurement sets. CALIPSO and CloudSat have been used to quantify the reliability of Moderate Resolution Imaging Spectroradiometer (MODIS) cloud products in both the Arctic and Antarctic. Looking at clouds over the Arctic Ocean, Liu *et al.* (2010) observe that the MODIS cloud accuracy is lower over ice, particularly in August–September when cloud frequency peaks (Intrieri *et al.*, 2002a; Dong *et al.*, 2010). The combined successful detection of both clouds and clear skies over open water is generally greater than 85% but this drops to less than 70% over sea-ice. A

similar reliability study of the CALIPSO and MODIS phase detection algorithms for clouds over Antarctica found agreement within 10% in cloud-top liquid water fraction (Choi *et al.*, 2010). However, the cloud-top liquid water fraction is not necessarily a good measure of total cloud liquid water, as the total column based on CALIOP profiles is 20–30% higher than the cloud-top fraction. This is seen in Figure 7 which shows the zonally-averaged liquid water fraction at cloud top and integrated throughout the cloud.

Recently a climatology of clouds and aerosols in the Arctic has been published, based on CALIOP measurements 2006–2010. Limiting the analysis to optically thin clouds, Devasthale *et al.* (2011a) reproduce, averaged over latitudes 67–82°N, the heavily skewed distribution in cloud base and thickness that has been seen in ground-based measurements (discussed in Section 7.2). Histograms of cloud-base height have a bimodal distribution which, as liquid- and ice-phase clouds are explicitly separated, show that the lower peak at 200–400 m is due to liquid clouds and that at 6–8 km is due to ice. Single layer clouds are most likely during all seasons which is not the same as clouds studied at SHEBA where the probability of multiple layers exceeded that of a single layer in June and July (Intrieri *et al.*, 2002a). There are two possibilities for the discrepancy, the most obvious is the point measurement of SHEBA compared to the spatially- and temporally-averaged CALIOP measurements, and the thin cloud requirement in the analysis by Devasthale *et al.* (2011a). Intrieri *et al.* (2002a) show that the greatest number of lidar-extinguishing clouds occur during summer, the combined radar-lidar technique being more resilient in these situations. A climatology of Arctic aerosols shows that 65% occurs in the lowest 1 km during winter, trapped by the surface temperature inversion. Increased vertical mixing occurs in the summer meaning that a single haze layer is most common with 45% being below 1 km (Devasthale *et al.*, 2011b). A comparison of the cloud and aerosol altitude distributions illustrates the significant overlay between Arctic haze and clouds with a significant liquid water content and the importance of understanding their interaction.

7. Summary of significant findings

The advantages of the lidar technique – the remote sensing of atmospheric constituents and processes at otherwise unobtainable temporal and spatial resolutions – have meant that, despite the difficulties of installation and operation, lidar measurements have played a significant role in increasing our understanding of the polar troposphere. In this section some of the historically significant steps are summarized.

7.1. Aerosols

7.1.1. Arctic haze

From the late 1970s through to the 1990s a substantial research effort was made to understand the winter and

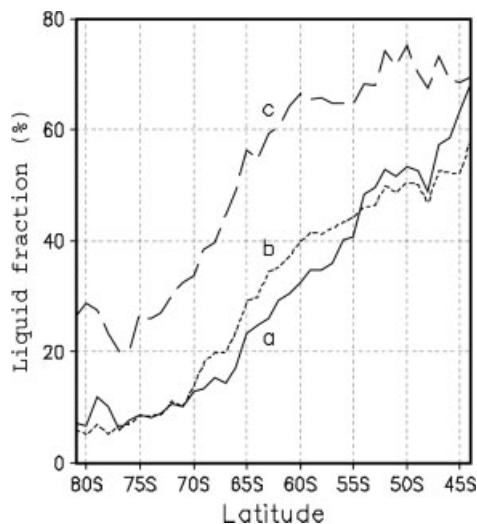


Figure 7. Antarctic zonally-averaged liquid water fraction for August 2006. Cloud-top fraction from MODIS (solid line, a) and CALIPSO (dotted line, b), and for the total cloud column from CALIPSO (dashed line, c) (from Choi *et al.*, 2010 with kind permission from Springer Science + Business Media).

spring-time occurrence of pervasive lower-tropospheric anthropogenic aerosols in the Arctic, termed Arctic haze (for a review see Quinn *et al.*, 2007). These fine-mode aerosols transported from mid-latitudes, have lifetimes of weeks in the stable winter time Arctic (Baskaran and Shaw, 2001). The haze is thickest in the lowest 2 km and may extend up to approximately 5 km. In late spring–early summer, aerosols also occur aloft with a clean air region at ground level, indicating more active transport from southern latitudes (Curry *et al.*, 2000). Brock *et al.* (2011) present an elegant discussion about characterizing Arctic haze as the seasonal maxima in the aerosol background and differentiating this from episodic aerosol events resulting from direct transport from lower latitudes. The terms ‘haze’ and ‘aerosol’ are used as strictly as possible in accordance with this definition, however the unequivocal separation of the two can be very difficult so care is required when studying this subject.

In spring 1983, a near-infrared lidar was flown from Ny-Ålesund to obtain backscatter profiles of the haze with vertical resolutions of 200 m (Wendling *et al.*, 1985). These were the first lidar measurements targeting Arctic haze and found aerosols concentrated within the boundary layer inversion (between the ground and 200–500 m) with backscatter coefficients peaking at $2.3\text{--}7 \times 10^{-5} \text{ m}^{-1} \text{ sr}^{-1}$. Hoff (1988) took the first depolarization measurements of Arctic haze, aerosols were differentiated from ice crystals using a total depolarization ratio of less than 0.1. This was subsequently refined by Ishii *et al.* (1999) who report seasonal average total depolarization ratios of 0.0088–0.0148 (converted from δ' to δ) for four winters at Eureka. The average backscatter ratio ranged from 1.21 to 1.29. A low depolarization ratio is expected due to the predominance of hygroscopic sea salts and sulphates in the haze (Quinn *et al.*, 2002)

although, as the depolarization ratio was greater than the calculated molecular ratio, aspherical particles still exert some influence on the optical properties. Hoffmann *et al.* (2009) report an average depolarization ratio for haze of 0.02–0.05 at Ny-Ålesund. The associated lidar ratios are 40–60 sr at 532/607 nm and 30–50 sr at 355/387 nm.

Using an aircraft-mounted lidar with a vertical resolution of only 3 m, Radke *et al.* (1989) show haze in the Canadian Arctic with fine vertical layered structures as small as tens of metres at altitudes up to the flight level of 4 km. Horizontal structure from 20 km for fine haze layers up to 500 km for thick, well mixed layers were seen. Similar structure was seen by Khatatov *et al.* (1997) down into the boundary layer in cases where a stable temperature inversion had formed. The highly-stratified haze is due to the stability of the Arctic boundary layer and contrasts with aerosol layers at lower latitudes that are both closer to the source regions and undergo greater mixing (Radke *et al.*, 1989; de Villiers *et al.*, 2010).

Along with the macrophysical and optical characteristics of haze, its chemical nature has been studied extensively. Due to the black carbon component, a slight surface cooling of $0.0\text{--}0.5 \text{ W m}^{-2}$ (Wendling *et al.*, 1985) was found in spring near Ny-Ålesund (and more generally $0.2\text{--}6 \text{ W m}^{-2}$, Quinn *et al.*, 2007 and references therein) due to solar absorption. During the winter, long wave radiation is enhanced. Aerosols have also been observed to modify the radiative contribution of thin clouds through the aerosol indirect effect (Garrett *et al.*, 2002; Lubin and Vogelmann, 2006).

7.1.2. Diamond dust

Clear-sky precipitation or diamond dust has long been a subject of interest in the polar regions due to the spectacular visual phenomena associated with its occurrence (Greenler, 1980). During the 1975 winter at the South Pole, where the 6 year winter-time average occurrence frequency of diamond dust is 63% (Walden *et al.*, 2003), Smiley and Morley (1981) found that layers generally form below the top of the temperature inversion and are capped by a separate ‘formation’ layer 75% of the time. Ice replicator studies revealed a predominance of simple crystal shapes; plates, prisms and bullets. The sizes given by Smiley and Morley (1981) were biased high due to the collection method, effective radii have more recently been measured at $12.2 \mu\text{m}$ in the winter (Walden *et al.*, 2003) and $17 \mu\text{m}$ in the summer (Lawson *et al.*, 2006).

Intrieri and Shupe (2004) present evidence of the radiative impact of diamond dust events on the surface, or more correctly the lack thereof, from measurements during SHEBA. Comparing observations to the radar and lidar data, they report that visual observations over-reported clear-sky precipitation events by almost 90% due to the presence of overlying sub-visible clouds. Separating the clear-sky events from the formation layer revealed that the radiative influence of the diamond dust itself is negligible. The source of the typically observed $20\text{--}40 \text{ W m}^{-2}$ enhancement in long wave surface flux is

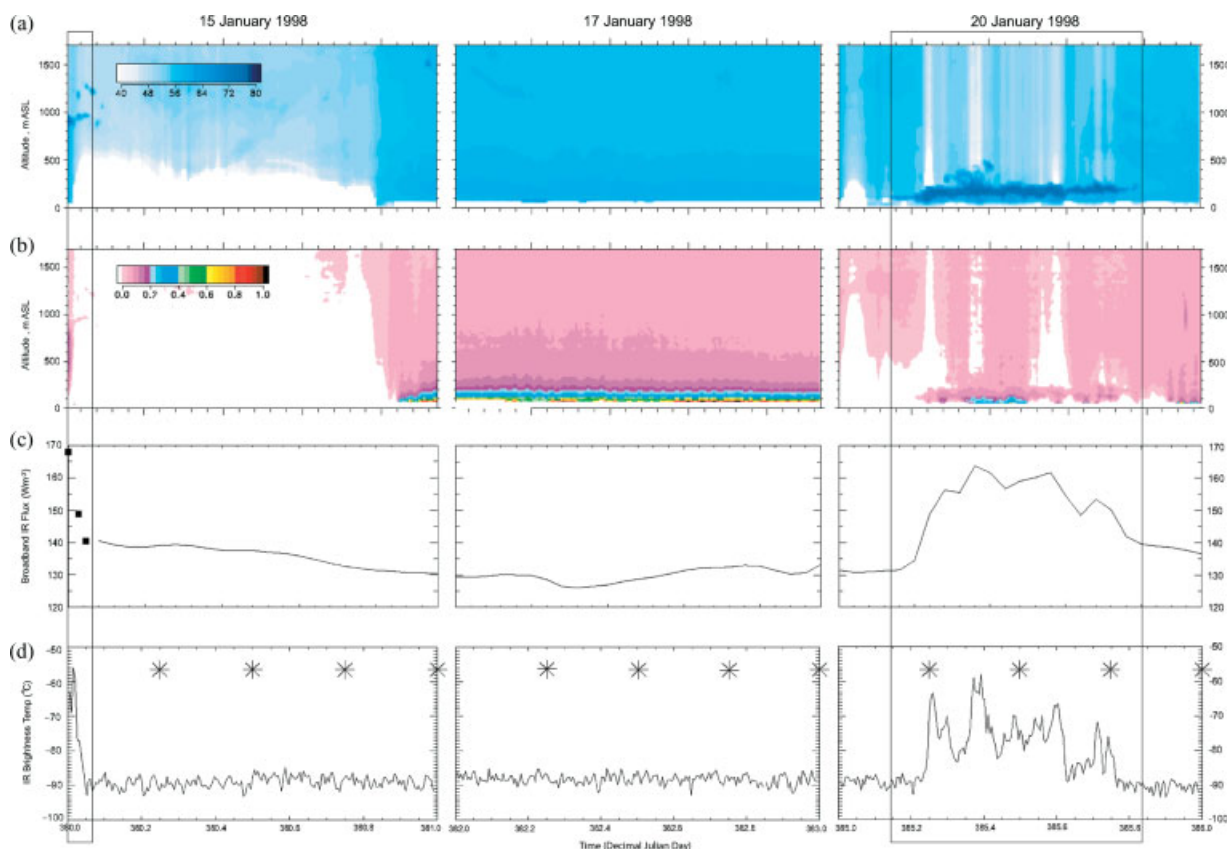


Figure 8. Lidar backscatter (a), and depolarization ratio (b), of instances of diamond dust recorded in January 1998 during SHEBA. Coincident long wave irradiance (c), and brightness temperatures (d), show that only when the ice crystals are associated with cloud (indicated with the black vertical lines) is the radiation affected (from Intrieri and Shupe, 2004).

thus the sub-visible clouds. This is illustrated in Figure 8 which shows measurements on three days. Only when a thin water cloud is present on 20 January, indicated by high backscatter and low depolarization ratios from the lidar, does the measured irradiance and brightness temperature increase. The diamond dust seen near the surface on the 17 January has no appreciable effect on the irradiance.

Diamond dust and Arctic haze both occur during the coldest months of the year in the lower troposphere. Sulphuric acid aerosols lower the homogeneous freezing temperature (Koop *et al.*, 1989) and concentration of ice nuclei (Borys, 1989) and may result in the formation of fewer and larger ice crystals (Grenier *et al.*, 2009). However, recent pan-polar investigations found little evidence of the inhibition of freezing due to the presence of sulphates (Grenier and Blanchet, 2010). It should be noted, however, that using CALIPSO and CloudSat data is complicated by limitations associated with isolating sulphate concentration and ice crystal size information from the aerosol and cloud data product.

7.2. Clouds

As mentioned in the context of the SHEBA measurements (Intrieri and Shupe, 2004), the accurate surface-based detection of clouds is greatly enhanced by using a lidar due to the extended periods of darkness and frequency of

optically thin clouds in the polar regions. Passive satellite cloud measurements also suffer due to the ambiguity between clouds and the high-albedo surface. Spinhirne *et al.* (2005), comparing cloud fractions over Antarctica in October 2003 from GLAS and MODIS, report discrepancies due to false positive cloud detections from MODIS of up to 40%. An accurate climatology of clouds, their altitude and microphysical properties is important due to their interaction with aerosols and radiation (Curry *et al.*, 1996). The lidar-derived depolarization ratio is arguably the most important instrument feature as it allows for the discrimination of pure liquid, ice and mixed-phase clouds and the cloud phase has a significant radiative impact on the surface (Shupe and Intrieri, 2004). For the majority of the year, with no solar radiation over the winter and a snow/ice covered (and thus high-albedo) surface, clouds have a positive forcing on the surface. Intrieri *et al.* (2002b) calculate a long wave forcing of approximately $+30 \text{ W m}^{-2}$ that dominates the total forcing except during the summer when the clouds increase the short wave albedo, resulting in a slight negative forcing. However, inhomogeneity of the surface albedo makes a quantitative determination difficult.

Tropospheric cloud cover is, as expected, strongly influenced by the proximity of the sea. The difference to mid-latitudes is that due to sea ice, the meteorology of a coastal site will display continental behaviour

during ice-bound winter months (Curry, 1983). The effect of the sea-ice on cloudiness in the Arctic is illustrated by Palm *et al.* (2010) who show spatial cloud fraction as measured by CALIPSO (averaged over $1^\circ \times 1^\circ$ gridboxes and so not immediately comparable to the temporal fractions measured at stationary sites) in antiphase with ice extent on the Arctic Ocean. Far from the coast, the South Pole has cloud occurrence frequencies of approximately 40% with little seasonal variation (Mahesh *et al.*, 2005). The cloud fraction is significantly higher at Syowa where Shiobara *et al.* (2003, adapted from Figure 5) show 2001 cloud fractions peaking at approximately 80% in the transition months and falling to a low of 32% during the winter. This is similar to a 1999–2004 lidar-radar climatology from Barrow where the average fraction was 78%, varying between approximately 60% in winter–spring and 90% in the autumn (Dong *et al.*, 2010). The cloud occurrence probability measured during the SHEBA campaign was very high, peaking in September at 97% while winter was the clearest season at 63% (Intrieri *et al.*, 2002a).

Cloud base heights in both the Arctic (Intrieri *et al.*, 2002a; Shiobara *et al.*, 2003) and Antarctic (Del Guasta *et al.*, 1993; Mahesh *et al.*, 2005) are heavily skewed in favour of low altitudes. A slight bimodal distribution is seen due to multi-layer clouds at the coastal sites although this is not seen in measurements at the South Pole (Del Guasta *et al.*, 1993). Intrieri *et al.* (2002a) show that multiple cloud layers are significantly less likely during the winter months. A climatology of non-extinguishing clouds over Dumont D'Urville reveals a mean geometric thickness around 3000 m at 230 K (Del Guasta *et al.*, 1993), although the values have been inflated as lidar-visible precipitation was also included in the cloud base. Colder clouds tend to be capped by the tropopause and so have a smaller vertical extent. In their CALIOP study, Palm *et al.* (2010) find that clouds over open water on average have a greater vertical extent, between 500 and 2000 m, compared to those over ice, although the authors do not detail how multiple layers were handled.

A collection of measured lidar ratios of Arctic clouds is given in Table I. Below, two particular topics of interest are discussed in more detail.

7.2.1. Mixed-phase clouds

Mixed-phase clouds consist of both ice and liquid water, although the vertical distribution of the phase is generally not uniform. Cloud tops are predominantly liquid while ice dominates at the cloud base (Raubert and Tokay, 1991), snow/virga is often seen beneath the cloud base. The distribution of liquid and ice and separation between cloud and precipitation can be determined due to the characteristic lidar signature of water compared to ice. Liquid water has a large backscatter signal and a depolarization ratio that approaches zero as liquid water fraction approaches 100%, an example is shown in Figure 5. Due to the large concentration of liquid cloud droplets, the elastic backscatter is very strong while the depolarization

is very low. Signals are sometimes totally extinguished inside the cloud layer making a complete parameterization of the cloud impossible without complementary radar profiles. For a thorough review of the state of mixed-phase clouds measurements from a range of instruments, see Shupe *et al.* (2008b).

These clouds are quite pervasive, measurements during SHEBA and at Barrow show that mixed-phase clouds respectively occur 55 and 59% of the time when clouds were detected (Shupe *et al.*, 2005). The mean cloud base height measured at Eureka over 2005–2007 was 680–2600 m with a small seasonal variation and this is similar to previous studies (de Boer *et al.*, 2009 and references therein). It should be noted that mixed-phase clouds were observed during SHEBA frequently to 4.5 km and occasionally up to 6.5 km (Intrieri *et al.*, 2002a). Cloud vertical extent averages 338 m but varies from tens of metres up to 1000 m (de Boer *et al.*, 2009). HSRL and cloud radar derived statistics of mixed-phase clouds at Barrow and Eureka are shown in Figure 9, note that multilayer mixed-phase clouds are not included and that the optical depth is skewed by the fact that clouds that completely extinguished the laser beam (approximately OD5) are also not included.

de Boer *et al.* (2011) presents a climatological occurrence probability distribution of tropospheric cloud types from Barrow (2004–2006), SHEBA, and Eureka (2005–2009), shown in Figure 10. Liquid clouds dominate for temperatures above ~ 265 K and ice clouds below ~ 245 K. In between these extremes, mixed-phase clouds are the most common cloud type. The fact that mixed-phase clouds occur over a very large range of temperatures accounts for their prevalence. The liquid water fraction increases slightly with temperature, although there are large variations between different studies (de Boer *et al.*, 2009 contains a summary of Arctic liquid water fractions). Using MODIS cloud-top temperature and phase retrieval, Choi *et al.* (2010) show a linear relationship between temperature and liquid water fraction over temperatures 250–260 K during the summertime Arctic (240–260 K for the Antarctic winter). However the uncertainties associated with the MODIS liquid water fraction were shown to be considerable when compared to that calculated from the CALIOP data as seen in Figure 7. Mixed-phase layers are often very stable, lasting for periods up to days. However, it has been observed that this stability may be temporarily disrupted through glaciation and sedimentation of the resulting ice crystals. Overlying cirrus has been observed to seed the glaciation of the mixed phase layer(s) in both the Antarctic summer (Morley *et al.*, 1989) and Arctic spring (Campbell and Shiobara, 2008). In both these cases, the mixed-phase layer reformed after the seed precipitation had ceased.

7.2.2. Ice crystal habit

Real clouds include a complex combination of habits, orientations, and phases, and a depolarization lidar is a powerful tool for their investigation. Noel *et al.* (2004)

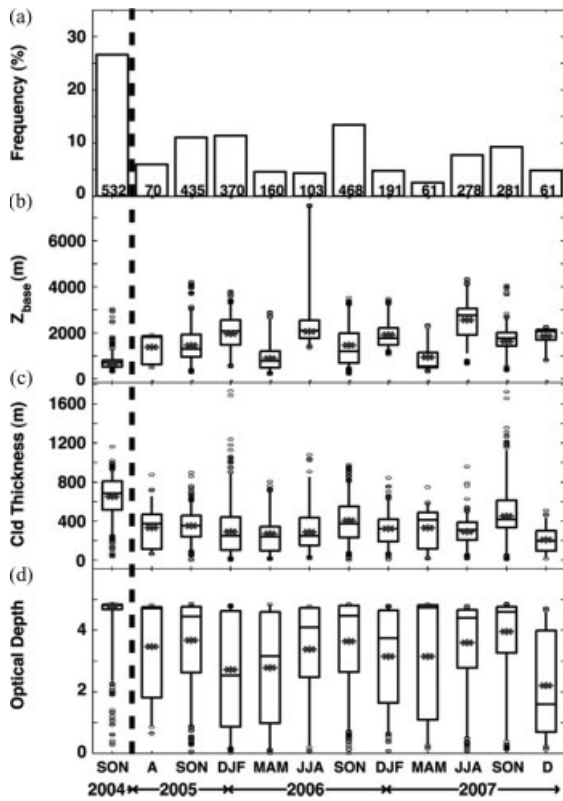


Figure 9. Macrophysical properties of single-layer mixed-phase clouds at Barrow (2004) and Eureka (2005–2007) derived from combined lidar-radar measurements. Shown are frequency of occurrence with number of cases included in the bar (a), mean cloud-base height (b), mean cloud vertical extent (c), and mean lidar-measured optical depth (d). The box-and-whisker plots provide the 5th, 25th, 50th, 75th, and 95th percentiles of 30 min averages, as well as the mean, *, and outer 10% of the data, ovals (from de Boer *et al.*, 2009).

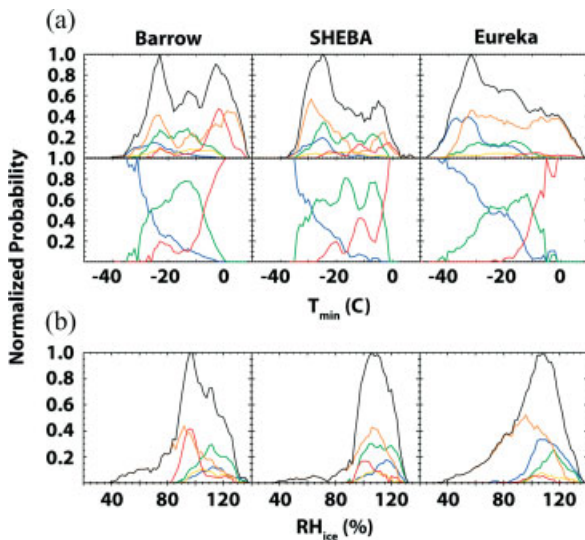


Figure 10. Normalized occurrence probability distributions of different cloud types as a function of temperature (a) and relative humidity (b) over ice for three Arctic sites. Distributions are for total cases (—), clear sky (—), ice clouds (—), liquid clouds (—), mixed-phase clouds topped by water (—), and ice-topped clouds with mixed-phase layers (—) (from de Boer *et al.*, 2011).

bin particle habit into three categories depending on lidar ratio: thin plates and spheroids for $\delta < 0.25$, columns for $\delta > 0.5$, and intermediate and irregular particles for $0.25 < \delta < 0.5$. This assumes a random orientation and difficulties arise when the ice crystals display a preferential orientation, generally a horizontal alignment. For a review of fall mechanisms and global measurements see Westbrook *et al.* (2010) and references therein. With a vertical-pointing lidar, strong specular reflections result, meaning there is enhanced backscatter and no depolarization. As a result, most depolarization lidars are pointed off vertical, an angle of 5° significantly reduces specular reflection while allowing for crystal flutter about the horizontal plane (Noel and Sassen, 2005).

The characteristic return from aligned ice crystals has been used to statistically classify cloud particles as randomly oriented or otherwise. The region of large backscatter and low depolarization data in Figure 6(a) is due to horizontally-aligned plates, this characteristic is significantly diminished once the lidar was pointed 3° off-nadir in November 2007. Sassen and Zhu (2009) find differences in cloud depolarization ratio of 0.04–0.05 ($\sim 10\%$ of total) at high latitudes indicating that aligned crystals are a minority of total crystal number concentration. However, temperature was not considered in this study and both Noel and Chepfer (2010) and Yoshida *et al.* (2010), using on-nadir measurements and statistical characterization as shown in Figure 6, contend that, although very small at low temperatures, for warmer clouds, >243 K for Noel and Chepfer (2010) and 265–255 K for Yoshida *et al.* (2010), the fraction of aligned to total ice crystals is approximately 50%. Westbrook *et al.* (2010) have done a similar, but importantly simultaneous, comparison of on- and off-zenith co-located lidars. Over 17 months they found that beneath liquid clouds between 260 and 245 K, more than 60% of the ice particles were horizontally aligned. This was for a mid-latitude site but as is seen in Figure 10, this temperature range also corresponds to a significant proportion of mixed-phase clouds in the Arctic.

It is interesting to compare these satellite measurements to available *in situ* cloud particle imager data. In doing so it should be noted that *in situ* measurements have been carried out only in the daylight months, and that the satellite studies are usually limited to optically thin clouds that do not extinguish the lidar beam. From the FIRE-ACE campaign data, Korolev *et al.* (1999) divides spring-time ice particles into pristine and irregular and finds that irregular ice dominated the studied clouds from 273 to 228 K (0.03–7.5 km) with a 97% occurrence frequency. Pristine ice peaked at 8% at the coldest temperatures, but even then thin plates were scarce. For a warm mixed-phase cloud (274–267 K at 0.55–1.7 km), Rangno and Hobbs (2001) report pristine, non-spherical, ice crystals accounted for 33% of all crystals. Needles were most prevalent at 18% while plates and short columns accounted for 3%. They point out that if

they classify identifiable rounded single crystals as irregular instead of pristine, as Korolev *et al.* (1999) do, they obtain a comparable ratio of irregular to pristine crystals.

More recently McFarquhar *et al.* (2007), averaging over three single-layer autumnal stratus clouds with mean mid-cloud temperatures around 260 K, found that spherical and semispherical particles dominate, particularly for the top half of the clouds. Of the ice in the lower half of the cloud, approximately 15% was needles and columns and 85% was irregular and rosettes (McFarquhar *et al.*, 2007, from figure 13). Gayet *et al.* (2009) report approximately 50% columns and plates at 253 K in a single spring-time mixed-phase cloud. At the South Pole, surface-based cloud particle imagers have been used for habit identification during the summer (Lawson *et al.*, 2006) and winter (Walden *et al.*, 2003). Despite complications due to wind-blown snow, with seasonal temperature ranges of 243–234 and 200–238 K respectively, these measurements provide a counter-point to the warm weather *in situ* measurements from the Arctic. In February 2001, columns and plates made up 45% of all crystals, 30% were rosettes, and 25% irregular shapes (mostly blowing snow). Measurements over June–September 1992 revealed relative proportions of 19% columns and plates, 1% rosettes, and 80% blown snow.

So the airborne *in situ* measurements tend not to support the hypothesis that aligned plates make up a significant proportion of the total cloud population. However, the *in situ* measurements over the Arctic have concentrated on spring–summer clouds and thus are perhaps not representative of the annual distribution of cloud particle types. Another issue is illustrated by FIRE.ACE measurements described by Hobbs *et al.* (2001); although proportions are not given, during a single flight 12 different clouds were sampled with widely varying crystal types. The vertical and horizontal variation in ice habit is expansive making comparisons between general satellite and specific *in situ* measurements difficult. Surface measurements on the Antarctic plateau however indicate that pristine crystals, and thus aligned plates under certain meteorological conditions, make up a considerable proportion of ice cloud particles.

With an assumption of randomly oriented ice crystals, one can convert between linear depolarization, δ_l , and circular, δ_c , through the relation $\delta_c = 2\delta_l/(1 - \delta_l)$ (Mishchenko and Hovenier, 1995). It is also possible to measure δ_l and δ_c separately and infer information about the scatterers based on the depolarization relationship. This is basis of the polarimetric lidar. Del Guasta *et al.* (2006) demonstrate such a lidar at mid-latitudes and find that for successful detection, comparable concentrations of aligned and random crystals were required. Also problematic is that simulations show that even small deformations to the ice crystals make discrimination between aligned and randomly-orientated crystals impossible. A similar system has recently been installed at Summit in Greenland, which measures linearly-polarized returns parallel, perpendicular, and at 45° to the transmitted beam

(Neely *et al.*, 2010). Another method for accessing scattering phase function information has been demonstrated at ALOMAR where Olofson *et al.* (2009) used a bistatic depolarization lidar. A bistatic system is one where the receiver is physically removed from the transmitter, in this case the receiver was 2.1 km distant. The receiver was scanned in the vertical plane to obtain height information, although this also changes the scattering angle. The limited dataset for a single cirrus cloud at 6.7 km did not allow the habit to be definitively determined, although results presented were consistent with those expected from columns with roughened edges.

7.3. Water vapour

Tropospheric water vapour mixing ratio measurements have been made at Ny-Ålesund since 2000 at both ultraviolet and visible wavelengths. Two case studies from winter 2002 are presented by Gerding *et al.* (2004) which show dramatic vertical and temporal changes in the water vapour field. Two distinct layers of aerosols are seen, the upper layer between 1 and 3.4 km displays a dramatic doubling of water vapour in a 3 h period. The lidar ratio for this period decreases from 60 to 45 sr which, along with back-trajectories of the sampled air masses, indicates anthropogenic aerosols that are swelling with the uptake of water. A second layer between the ground and 1 km exhibits a similar increase in water vapour mixing ratio throughout the day, however the lidar ratio of 10 sr remains constant. The authors conclude that the aerosols in the boundary layer are most probably sea salt particles or ice crystals. The second case study illustrated the influence of local topography and wind direction on the water vapour mixing ratio in the lowest 1 km.

Very similar structures in the water vapour field have been observed at Eureka. One episode in February 2010 was studied both vertically with a lidar and horizontally with satellite measurements of precipitable water (Doyle *et al.*, 2011). The lidar measurement is shown in Figure 11 and the increases in water vapour seen at 0300 UTC 9 February and 1200 UTC 10 February are

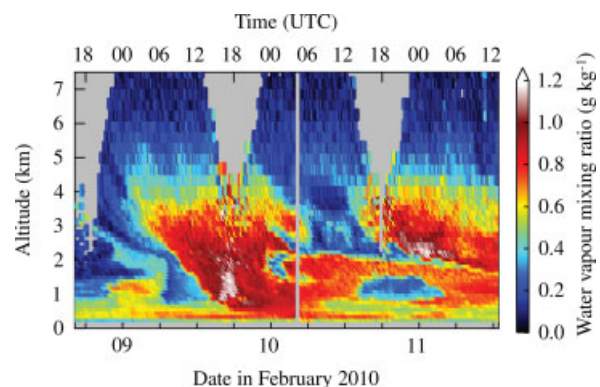


Figure 11. Water vapour mixing ratio measured at Eureka, February 2010. Gray regions indicate invalid or missing data (adapted from Doyle *et al.*, 2011).

attributed to a moist air mass that originated in the north Pacific Ocean and swept up into the Arctic. Measurements of long wave downwelling irradiance showed that water vapour alone contributed an additional 13 W m^{-1} to the irradiance during the peak of this water vapour intrusion.

7.4. Ozone

Ozone lidars have been used to measure temporal, vertical and horizontal distributions of tropospheric ozone in the Arctic and to obtain climatological trends with both season and latitude. Tropospheric ozone levels tend to increase during spring and into summer as solar heating breaks down the stable boundary layer and transport from more southerly latitudes increases (Browell *et al.*, 2003). In summer 1988, twin upward- and downward-looking ozone lidars were flown across Greenland, Canada, and Alaska (Browell *et al.*, 1992). The average background concentration seen was 29 ppbv at 500 m with a concentration gradient of 5.2 ppbv km^{-1} . Thirty eight percent of the sampled troposphere north of 65°N was influenced by stratospheric intrusions during which ozone levels could be elevated to $>100 \text{ ppbv}$ in the mid-troposphere. The boundary layer over regions of open water had a higher aerosol loading and slightly elevated ozone levels compared to that over the tundra, indicating a possible ozone sink over the land.

Surface-based sudden ozone depletion events are related to the photochemical reaction of the ozone with bromine and other sea salt-derived species (Simpson *et al.*, 2007) and have been studied extensively in the Arctic since the 1980s and less so in the Antarctic (Wessel *et al.*, 1998). Measurements of vertical structure have primarily relied on ozonesondes. Sondes may be launched when surface measurements indicate a depletion is in process (Wessel *et al.*, 1998) or regularly on a 12 hourly basis (Bottenheim *et al.*, 2002). With ozone depletion events lasting from less than a day up to several days, this is hardly ideal. DIAL measurements provide the required temporal resolution to characterize the dynamics of these events. The depletions are generally confined to the boundary layer and although they have been seen detached from the surface (Bottenheim *et al.*, 2002), this is the exception. Using aerosol along with the ozone channels, measurements by Browell *et al.* (2003) indicate that the ozone depletion events also exhibit an enhanced backscatter ratio, although *in situ* measurements remain conflicting (see the TOPSE experiment in Section 5.8 for details).

8. Future directions

Since the 1970s lidars have been used to characterize the polar atmosphere and have added extensively to the knowledge of these regions. Below are some areas that the authors believe warrant attention and present possible future directions for lidar measurements at the poles.

With the cost of installation and operation very high, system capability shall increase to maximize the return on investment. This has already occurred in terms of synergy between different types of instruments, it is now unusual to see a lidar not accompanied by a radar, photometer, radiometer, or other instruments, and lidar systems themselves will become increasingly complex. This will improve the study of interaction between aerosols and clouds and other species. Profiles also complement wide-area satellite column measurements, for example water vapour profiles at Eureka and precipitable water from the Microwave Humidity Sounder instruments (Doyle *et al.*, 2011). There are now four water vapour tropospheric lidars in the Arctic with ALOMAR adding an ultraviolet water vapour channel to their tropospheric lidar in summer 2011 (M. Gausa, personal communication). With the addition of temperature, relative humidity can be measured and this could be a significant step. It will allow the examination of the interaction between hydrometeors and aerosols, for example the sulphate-induced freezing inhibition effect (Grenier and Blanchet, 2010) and more detailed studies of cloud formation processes.

With CALIOP, the usefulness of new elastic aerosol micropulse systems seems questionable. Such systems could be superseded by micropulse water vapour or ozone DIAL technology currently being developed (Wirth *et al.*, 2009) that also provide aerosol products. However, there are two possible exceptions: (1) facilities concentrating on long term data records for the detection of changes in climate such as those at NDACC sites, and, (2) to cover gaps in satellite coverage. Spatially, these are locations close to the poles. Temporally, it is important to consider that the original CALIPSO mission ended in June 2009 and despite its continuing successes at some point the instrument will fail. Several new lidar platforms are being developed to extend the capabilities of global lidar measurements. Most relevant are the cloud and aerosol lidars being developed by ESA with the ATmospheric LIDar (ATLID on the EarthCARE satellite, scheduled launch 2015), and NASA with the Aerosol-Cloud-Ecosystems (ACE, scheduled launch 2013–2016) instrument. Both of these are high-spectral resolution lidars and so will measure extinction and backscatter coefficients independently along with depolarization. Studies are ongoing into a satellite-borne water vapour DIAL although they are currently limited to an aircraft-mounted demonstrator (Browell *et al.*, 1998; Wirth *et al.*, 2009) and so not slated for a satellite mission in the immediate future.

The issues relating to cloud ice crystal habit are still of major concern, as the habit, with all its complexity within and between clouds, has a significant impact on a cloud's radiative influence (Key *et al.*, 2002). Polarimetric lidar techniques rely on understanding the scattering phase function of the crystals being investigated, something that is complicated by roughened or rounded crystals as well as the range of crystal shapes within the sampled volume (Del Guasta *et al.*, 2006). *In situ* measurements are necessary, particularly during the winter as aircraft campaigns up to now have concentrated on the

'light' months, partly due to the interest in springtime processes and partly because of the risks associated with wintertime flights. At Ny-Ålesund a tethered balloon with meteorological package, radiometers and a cloud particle imager takes profiles during controlled ascents to 1.2 km (Sikand *et al.*, 2010). At the time of writing only radiometric data have been published, however the imager should prove a useful companion to the depolarization lidar at Ny-Ålesund.

Lidar technology has allowed for the remote sensing of the polar atmosphere with unprecedented precision since the 1970s. Despite the advances in access and technology, active tropospheric lidars are still in very limited numbers at high latitudes. Lidars are now located alongside other atmospheric instruments, both active and passive, increasing the scientific payoff of what are complicated and expensive instruments. As technologies are proven at mid-latitudes and pushed into the polar regions, lidars will continue to prove themselves invaluable in understanding the processes that govern the polar troposphere.

Acknowledgements

C. Ritter and R. Neuber very kindly shared some of the challenges of operating in the Arctic. The authors thank G. Lesins, N. T. O'Neill, J. R. Pierce, and two referees for valuable feedback on the manuscript. GJN acknowledges the financial support of the Canadian Network for the Detection of Atmospheric Change (CANDAC).

References

- Adachi H, Shibata T, Iwasaka Y, Fujiwara M. 2001. Calibration method for the lidar-observed stratospheric depolarization ratio in the presence of liquid aerosol particles. *Applied Optics* **40**: 6587–6595.
- Adriani A, Massoli P, Di Donfrancesco G, Cairo F, Moriconi ML, Snels M. 2004. Climatology of polar stratospheric clouds based on lidar observations from 1993 to 2001 over McMurdo Station, Antarctica. *Journal of Geophysical Research* **109**: D24211, DOI: 10.1029/2004JD004800.
- Ansmann A, Müller D. 2005. Lidar and atmospheric aerosol particles. In *Lidar: Range-Resolved Optical Remote Sensing of the Atmosphere*, Weitkamp C (ed.). Springer: Singapore; 105–141.
- Ansmann A, Riebesell M, Wandinger U, Weitkamp C, Voss E, Lahmann W, Michaelis W. 1992. Combined Raman elastic-backscatter LIDAR for vertical profiling of moisture, aerosol extinction, backscatter, and LIDAR ratio. *Applied Physics B* **55**: 18–28.
- Arctic Haze. 1997. *Atmospheric Research* **44**: 1–230. (special issue).
- Atlas EL, Ridley BA, Cantrell CA. 2003. The tropospheric ozone production about the spring equinox (TOPSE) experiment: introduction. *Journal of Geophysical Research* **108**: 8353, DOI: 10.1029/2002JD003172.
- Baskaran M, Shaw GE. 2001. Residence time of arctic haze aerosols using the concentrations and activity ratios of ^{210}Po , ^{210}Pb and ^7Be . *Journal of Aerosol Science* **32**: 443–452.
- Behrendt A. 2005. Temperature measurements with lidar. In *Lidar: Range-Resolved Optical Remote Sensing of the Atmosphere*, Weitkamp C (ed.). Springer: Singapore; 273–305.
- Bodhaine BA, Wood NB, Dutton EG, Slusser JR. 1999. On Rayleigh optical depth calculations. *Journal of Atmospheric and Oceanic Technology* **16**: 1854–1861.
- de Boer G, Eloranta EW, Shupe MD. 2009. Arctic mixed-phase stratiform cloud properties from multiple years of surface-based measurements at two high-latitude locations. *Journal of Atmospheric Sciences* **66**: 2874–2887.
- de Boer G, Morrison H, Shupe MD, Hildner R. 2011. Evidence of liquid dependent ice nucleation in high-latitude stratiform clouds from surface remote sensors. *Geophysical Research Letters* **38**: L01803, DOI: 10.1029/2010GL046016.
- Bony S, Colman R, Kattsov VM, Allan RP, Bretherton CS, Dufresne J-L, Hall A, Hallgatte S, Holland MM, Ingram W, Randall DA, Soden BJ, Tselioudis G, Webb MJ. 2006. How well do we understand and evaluate climate change feedback processes? *Journal of Climate* **19**: 3445–3482.
- Borys RD. 1989. Studies of ice nucleation by arctic aerosols on AGASP-II. *Journal of Atmospheric Chemistry* **9**: 169–185.
- Bottenheim JW, Fuentes JD, Tarasick DW, Anlauf KG. 2002. Ozone in the arctic lower troposphere during winter and spring 2000 (ALERT2000). *Atmospheric Environment* **36**: 2535–2544.
- Bourdages L, Duck TJ, Lesins G, Eloranta EW. 2009. Physical properties of high arctic tropospheric particles during winter. *Atmospheric Chemistry and Physics* **9**: 6881–6897.
- Brock CA, Cozic J, Bahreini R, Froyd KD, Middlebrook AM, McComiskey A, Brioude J, Cooper OR, Stohl A, Aikin KC, de Gouw JA, Fahey DW, Ferrare RA, Gao R-S, Gore W, Holloway JS, Hübler G, Jefferson A, Lack DA, Lance S, Moore RH, Murphy DM, Nenes A, Novelli PC, Nowak JB, Ogren JA, Peischl J, Pierce RB, Pilewskie P, Quinn PK, Ryerson TB, Schmidt KS, Schwarz JP, Sodemann H, Spackman JR, Stark H, Thomson DS, Thornberry T, Veres P, Watts LA, Warneke C, Wollny AG. 2011. Characteristics, sources, and transport of aerosols measured in spring 2008 during the aerosol, radiation, and cloud processes affecting Arctic climate (ARCPAC) project. *Atmospheric Chemistry and Physics* **11**: 2423–2453.
- Brock CA, Radke LF, Hobbs PV. 1990. Sulfur in particles in Arctic hazes derived from airborne in situ and lidar measurements. *Journal of Geophysical Research* **95**(22): 22369–22387.
- Browell EV, Butler CF, Kooi SA, Fenn MA, Harriss RC, Gregory GL. 1992. Large-scale variability of ozone and aerosols in the summertime Arctic and sub-Arctic troposphere. *Journal of Geophysical Research* **97**(16): 16433–16450.
- Browell EV, Hair JW, Butler CF, Grant WB, DeYoung RJ, Fenn MA, Brackett VG, Clayton MB, Brasseur LA, Harper DB, Ridley BA, Klonecki AA, Hess PG, Emmons LK, Tie XX, Atlas EL, Cantrell CA, Wimmers AJ, Blake DR, Coffey MT, Hannigan JW, Dibb JE, Talbot RW, Flocke F, Weinheimer AJ, Fried A, Wert B, Snow JA, Lefer BL. 2003. Ozone, aerosol, potential vorticity, and trace gas trends observed at high-latitudes over North America from February to May 2000. *Journal of Geophysical Research* **108**: 8369, DOI: 10.1029/2001JD001390.
- Browell EV, Ismail S, Grant WB. 1998. Differential absorption lidar (DIAL) measurements from air and space. *Applied Physics B* **67**: 399–410.
- Budikova D. 2009. Role of Arctic sea ice in global atmospheric circulation: a review. *Global and Planetary Change* **68**: 149–163.
- CALIPSO. 2009. *Journal of Atmospheric and Oceanic Technology* **10–11** (special issue).
- Campbell JR, Shiobara M. 2008. Glaciation of a mixed-phase boundary layer cloud at a coastal arctic site as depicted in continuous lidar measurements. *Polar Science* **2**: 121–127.
- Castagnoli MDF, Vitale V. 2010. An automated lidar for the monitoring of tropospheric clouds and aerosols at Concordia Station (Antarctica). *Proceedings of 25th International Laser Radar Conference*, St. Petersburg; 1130–1133.
- Choi Y-S, Ho C-H, Kim S-W, Lindzen RS. 2010. Observational diagnosis of cloud phase in the winter Antarctic atmosphere for parameterizations in climate models. *Advances in Atmospheric Sciences* **27**: 1233–1245.
- Cooney J. 1972. Measurement of atmospheric temperature profiles by Raman backscatter. *Journal of Applied Meteorology* **11**: 108–112.
- Curry J. 1983. On the formation of continental polar air. *Journal of Aerosol Science* **40**: 2278–2292.
- Curry JA, Ebert EE. 1992. Annual cycle of radiation fluxes over the Arctic Ocean: sensitivity to cloud optical properties. *Journal of Climate* **5**: 1267–1280.
- Curry JA, Hobbs PV, King MD, Randall DA, Minnis P, Isaac GA, Pinto JO, Uttal T, Bucholtz A, Cripe DG, Gerber H, Fairall CW, Garrett TJ, Hudson J, Intrieri JM, Jakob C, Jensen T, Lawson P, Marcotte D, Nguyen L, Pilewskie P, Rangno A, Rogers DC, Strawbridge KB, Valero FPJ, Williams AG, Wylie D. 2000. FIRE Arctic clouds experiment. *Bulletin of the American Meteorological Society* **81**: 5–29.
- Curry JA, Rossow WB, Randall D, Schramm JL. 1996. Overview of Arctic cloud and radiation characteristics. *Journal of Climate* **9**: 1731–1764.
- Curry JA, Schramm JL, Ebert EE. 1995. Sea ice-albedo climate feedback mechanism. *Journal of Climate* **8**: 240–247.

- Del Guasta M, Morandi M, Stefanutti L, Brechet J, Piquad J. 1993. One year of cloud lidar data from Dumont d'Urville (Antarctica) 1. General overview of geometrical and optical properties. *Journal of Geophysical Research* **98**(18): 18575–18587.
- Del Guasta M, Vallar E. 2003a. In-cloud variability of lidar depolarization of polar and midlatitude cirrus. *Geophysical Research Letters* **30**: 1578, DOI: 10.1029/2003GL017163.
- Del Guasta M, Vallar E. 2003b. Correction to "In-cloud variability of lidar depolarization of polar and midlatitude cirrus". *Geophysical Research Letters* **30**: 1838, DOI: 10.1029/2003GL018214.
- Del Guasta M, Vallar E, Riviere O, Castagnoli F, Venturi V, Morandi M. 2006. Use of polarimetric lidar for the study of oriented ice plates in clouds. *Applied Optics* **45**: 4878–4887.
- Devasthale A, Tjernström M, Karlsson K-G, Thomas MA, Jones C, Sedlar J, Omar AH. 2011a. The vertical distribution of thin features over the Arctic analysed from CALIPSO observations part I: optically thin clouds. *Tellus* **63B**: 77–85.
- Devasthale A, Tjernström M, Omar AH. 2011b. The vertical distribution of thin features over the Arctic analysed from CALIPSO observations part II: aerosols. *Tellus* **63B**: 86–95.
- Di Donfrancesco G, Adriani A, Gobbi GP, Cairo F. 2000. Lidar observations of the stratospheric aerosol during 1993 above McMurdo Station, Antarctica. *Journal of Atmospheric and Solar-Terrestrial Physics* **62**: 713–723.
- Dong X, Xi B, Crosby K, Long CN, Stone RS, Shupe MD. 2010. A 10 year climatology of Arctic cloud fraction and radiative forcing at Barrow, Alaska. *Journal of Geophysical Research* **115**: D17212, DOI: 10.1029/2009JD013489.
- Donovan DP, Bird JC, Whiteway JA, Duck TJ, Pal SR, Carswell AI. 1995. Lidar observations of stratospheric ozone and aerosol above the Canadian High Arctic during the 1994–95 winter. *Geophysical Research Letters* **22**: 3489–3492.
- Doyle JG, Lesins G, Thackray CP, Perro C, Nott GJ, Duck TJ, Damoah R, Drummond JR. 2011. Water vapor intrusions into the high Arctic during winter. *Geophysical Research Letters* **38**: L12806, DOI: 10.1029/2011GL047493.
- Eloranta EW, Razenkov IA, Garcia JP. 2006. Arctic observations with the University of Wisconsin high spectral resolution lidar. *Proceedings of 23rd International Laser Radar Conference*, Nara; 399–402.
- Ferrare RA, Melfi SH, Whiteman DN, Evans KD, Schmidlin FJ, Starr DO. 1995. A comparison of water vapor measurements made by Raman lidar and radiosondes. *Journal of Atmospheric and Oceanic Technology* **12**: 1177–1195.
- Fiocco G, Smullin LD. 1963. Detection of scattering layers in the upper atmosphere (60–140 km) by optical radar. *Nature* **199**: 1275–1276.
- Francis JA, Chan W, Leathers DJ, Miller JR, Veron DE. 2009. Winter Northern Hemisphere weather patterns remember summer Arctic sea-ice extent. *Geophysical Research Letters* **36**: L07503, DOI: 10.1029/2009GL037274.
- Frioud M, Gausa M, Baumgarten G, Kristjansson JE, Førre I. 2006. New tropospheric lidar system in operation at ALOMAR (69°N, 16°E). *Proceedings of 23rd International Laser Radar Conference*, Nara; 179–182.
- Garrett TJ, Radke LF, Hobbs PV. 2002. Aerosol effects on cloud emissivity and surface long wave heating in the Arctic. *Journal of Atmospheric Sciences* **59**: 769–778.
- Gayet J-F, Mioche G, Dörnbrack A, Ehrlich A, Lampert A, Wendisch M. 2009. Microphysical and optical properties of Arctic mixed-phase clouds. The 9 April 2007 case study. *Atmospheric Chemistry and Physics* **9**: 6581–6595.
- Gayet J-F, Stachlewska IS, Jourdan O, Shcherbakov V, Schwarzenboeck A, Neuber R. 2007. Microphysical and optical properties of precipitating drizzle and ice particles obtained from alternated lidar and in situ measurements. *Annales Geophysicae* **25**: 1487–1497.
- Gerding M, Ritter C, Müller M, Neuber R. 2004. Tropospheric water vapour soundings by lidar at high Arctic latitudes. *Atmospheric Research* **71**: 289–302.
- Gillett NP, Stone DA, Stott PA, Nozawa T, Karpechko AY, Hegerl GC, Wehner MF, Jones PD. 2008. Attribution of polar warming to human influence. *Nature Geoscience* **1**: 750–754.
- Greenler R. 1980. *Rainbows, Halos, and Glories*. Cambridge University Press: New York, NY.
- Grenier P, Blanchet J-P. 2010. Investigation of the sulphate-induced freezing inhibition effect from CloudSat and CALIPSO measurements. *Journal of Geophysical Research* **115**: D22205, DOI: 10.1029/2010JD013905.
- Grenier P, Blanchet J-P, Muñoz-Alpizar R. 2009. Study of polar thin ice clouds and aerosols seen by CloudSat and CALIPSO during midwinter 2007. *Journal of Geophysical Research* **114**: D09201, DOI: 10.1029/2008JD010927.
- Gultepe I, Isaac GA, Williams A, Marcotte D, Strawbridge KB. 2003. Turbulent heat fluxes over leads and polynyas, and their effects on Arctic clouds during FIRE. ACE: aircraft observations for April 1998. *Atmosphere-Ocean* **41**: 15–34.
- Harris RC, Wofsy SC, Bartlett DS, Shipham MC, Jacob DJ, Hoell JM Jr, Bendura RJ, Drewry JW, McNeal RJ, Navarro RL, Gidge RN, Rabine VE. 1992. The arctic boundary layer expedition (ABLE 3A): July–August 1988. *Journal of Geophysical Research* **97**(16): 16383–16394.
- Hauchecorne A, Chanin M-L. 1980. Density and temperature profiles obtained by lidar between 35 and 70 km. *Geophysical Research Letters* **7**: 565–568.
- Hobbs PV, Rangno AL, Shupe M, Uttal T. 2001. Airborne studies of cloud structures over the Arctic Ocean and comparisons with retrievals from ship-based remote sensing measurements. *Journal of Geophysical Research* **106**(15): 15029–15044.
- Hoff RM. 1988. Vertical structure of Arctic haze observed by lidar. *Journal of Applied Meteorology* **27**: 125–139.
- Hoffmann A, Ritter C, Neuber R, Beninga I, Schmid J. 2010. A redesigned Raman lidar for cloud and aerosol profiling in the Arctic. *Proceedings of 25th International Laser Radar Conference*, St. Petersburg; 75–78.
- Hoffmann A, Ritter C, Stock M, Shiobara M, Lampert A, Maturilli M, Orgis T, Neuber R, Herber A. 2009. Ground-based lidar measurements from Ny-Ålesund during ASTAR 2007. *Atmospheric Chemistry and Physics* **9**: 9059–9081.
- Hu Y, Vaughan M, Liu Z, Lin B, Yang P, Flittner D, Hunt B, Kuehn R, Huang J, Wu D, Rodier S, Powell K, Trepte C, Winker D. 2007. The depolarization-attenuated backscatter relation: CALIPSO lidar measurements vs. theory. *Optics Express* **15**: 5327–5332.
- Hu Y, Winker D, Vaughan M, Lin B, Omar A, Trepte C, Flittner D, Yang P, Nasiri SL, Baum B, Holz R, Sun W, Liu Z, Wang Z, Young S, Stamnes K, Huang J, Kuehn R. 2009. CALIPSO/CALIP cloud phase discrimination algorithm. *Journal of Atmospheric and Oceanic Technology* **26**: 2293–2309.
- Intrieri JM, Fairall CW, Shupe MD, Persson POG, Andreas EL, Guest PS, Moritz RE. 2002b. An annual cycle of Arctic surface cloud forcing at SHEBA. *Journal of Geophysical Research* **107**: 8039, DOI: 10.1029/2000JC000439.
- Intrieri JM, Shupe MD. 2004. Characteristics and radiative effects of diamond dust over the western Arctic Ocean region. *Journal of Climate* **17**: 2953–2960.
- Intrieri JM, Shupe MD, Uttal T, McCarty BJ. 2002a. An annual cycle of Arctic cloud characteristics observed by radar and lidar at SHEBA. *Journal of Geophysical Research* **107**: C10, DOI: 10.1029/2000JC000423.
- Ishii S, Shibata T, Nagai T, Mizutani K, Itabe T, Hirota M, Fujimoto T, Uchino O. 1999. Arctic haze and clouds observed by lidar during four winter seasons of 1993–1997, at Eureka, Canada. *Atmospheric Environment* **33**: 2459–2470.
- Iwasaka Y. 1985. Lidar measurement of the stratospheric aerosol layer at Syowa Station (69.00°S, 39.35°E), Antarctica. *Journal of the Meteorological Society of Japan* **63**: 283–287.
- Jacob DJ, Crawford JH, Maring H, Clarke AD, Dibb JE, Emmons LK, Ferrare RA, Hostetler CA, Russell PB, Singh HB, Thompson AM, Shaw GE, McCauley E, Pederson JR, Fisher JA. 2010. The Arctic Research of the Composition of the Troposphere from Aircraft and Satellites (ARCTAS) mission: design, execution, and first results. *Atmospheric Chemistry and Physics* **10**: 5191–5212.
- Key JR, Yang P, Baum BA, Nasiri SL. 2002. Parameterization of short wave ice cloud optical properties for various particle habits. *Journal of Geophysical Research* **107**: D13, DOI: 10.1029/2001JD000742.
- Khattatov VU, Tyabotov AE, Alekseyev AP, Postnov AA, Stulov EA. 1997. Aircraft lidar studies of the Arctic haze and their meteorological interpretation. *Atmospheric Research* **44**: 99–111.
- Klein SA, McCoy RB, Morrison H, Ackerman AS, Avramov A, de Boer G, Chen M, Cole JNS, Del Genio AD, Falk M, Foster MJ, Fridlind A, Golaz J-C, Hashino T, Harrington JY, Hoose C, Khairoutdinov MF, Larson VE, Liu X, Luo Y, McFarquhar GM, Menon S, Neggers RAJ, Park S, Poellot MR, Schmidt JM, Sednev I, Shipway BJ, Shupe MD, Spangenberg DA, Sud YC, Turner DD, Veron DE, von Salzen K, Walker GK, Wang Z, Wolf AB, Xie S, Xu K-M, Yang F, Zhang G. 2009. Intercomparison of model simulations of mixed-phase clouds observed during the ARM Mixed-Phase Arctic Cloud Experiment. I: single-layer cloud. *Quarterly Journal of the Royal Meteorological Society* **135**: 979–1002.

- Koop T, Ng HP, Molina LT, Molina MJ. 1989. A new optical technique to study aerosol phase transitions: the nucleation of ice from H₂SO₄ aerosols. *Journal of Physical Chemistry A* **102**: 8924–8931.
- Korolev AV, Isaac GA, Hallett J. 1999. Ice particle habits in Arctic clouds. *Geophysical Research Letters* **26**: 1299–1302.
- Lampert A, Ehrlich A, Dörnbrack A, Jourdan O, Gayet J-F, Mioche G, Shcherbakov V, Ritter C, Wendisch M. 2009. Microphysical and radiative characterization of a subvisible midlevel Arctic ice cloud by airborne observations a case study. *Atmospheric Chemistry and Physics* **9**: 2647–2661.
- Lampert A, Ritter C, Hoffmann A, Gayet JF, Mioche G, Ehrlich A, Doernbrack A, Wendisch M, Shiobara M. 2010. Lidar characterization of the Arctic atmosphere during ASTAR 2007: four cases studies of boundary layer, mixed-phase and multi-layer clouds. *Atmospheric Chemistry and Physics* **10**: 2847–2866.
- Lawson RP, Baker BA, Zmarzly P, O'Connor D, Mo Q, Gayet J-F, Shcherbakov V. 2006. Microphysical and optical properties of atmospheric ice crystals at South Pole Station. *Journal of Applied Meteorology and Climatology* **45**: 1505–1524.
- Leaitch WR, Hoff RM, MacPherson JI. 1987. Airborne and lidar measurements of aerosol and cloud particles in the troposphere over Alert Canada in April 1986. *Journal of Atmospheric Chemistry* **9**: 187–211.
- Lesins G, Duck TJ, Drummond JR. 2010. Climate trends at Eureka in the Canadian high Arctic. *Atmosphere-Ocean* **48**: 59–80.
- Liu Y, Ackerman SA, Maddux BC, Key JR, Frey RA. 2010. Errors in cloud detection over the Arctic using a satellite imager and implications for observing feedback mechanisms. *Journal of Climate* **23**: 1894–1907.
- Liu L, Mishchenko MI. 2001. Constraints on PSC particle microphysics derived from lidar observations. *Journal of Quantitative Spectroscopy and Radiative Transfer* **70**: 817–831.
- Lubin D, Vogelmann AM. 2006. A climatologically significant aerosol long wave indirect effect in the Arctic. *Nature* **439**: 453–456.
- McCormick MP, Steele HM, Hamill P, Chu WP, Swissler TJ. 1982. Polar stratospheric cloud sightings by SAM II. *Journal of Atmospheric Sciences* **39**: 1387–1397.
- McFarquhar GM, Zhang G, Poellot MR, Kok GL, McCoy R, Tooman T, Fridlind A, Heymsfield AJ. 2007. Ice properties of single-layer stratocumulus during the Mixed-Phase Arctic Cloud Experiment: 1. Observations. *Journal of Geophysical Research* **112**: D24201, DOI: 10.1029/2007JD008633.
- McGill M, Hlavka D, Hart W, Scott VS, Spinhirne J, Schmid B. 2002. Cloud physics lidar: instrument description and initial measurement results. *Applied Optics* **41**: 3725–3734.
- Mahesh A, Campbell JR, Spinhirne JD. 2005. Multi-year measurements of cloud base heights at South Pole by lidar. *Geophysical Research Letters* **32**: L09812, DOI: 10.1029/2004GL021983.
- Mahesh A, Eager R, Campbell JR, Spinhirne JD. 2003. Observations of blowing snow at the South Pole. *Journal of Geophysical Research* **108**: 4707, DOI: 10.1029/2002JD003327.
- Mishchenko MI, Hovenier JW. 1995. Depolarization of light backscattered by randomly oriented nonspherical particles. *Optics Letters* **20**: 1356–1358.
- Moritz RE, Bitz CM, Steig EJ. 2002. Dynamics of recent climate change in the Arctic. *Science* **297**: 1497–1502.
- Morley BM, Uthe EE, Viezee W. 1989. Airborne lidar observations of clouds in the Antarctic troposphere. *Geophysical Research Letters* **16**: 491–494.
- Morley BM, Uthe EE, Viezee W. 1990. Airborne lidar observations during AGASP-2. *Journal of Applied Meteorology* **29**: 268–271.
- Morrison H, McCoy RB, Klein SA, Xie S, Luo Y, Avramov A, Chen M, Cole JNS, Falk M, Foster MJ, Del Genio AD, Harrington JY, Hoose C, Khairoutdinov MF, Larson VE, Liu X, McFarquhar GM, Poellot MR, von Salzen K, Shipway BJ, Shupe MD, Sud YC, Turner DD, Veron DE, Walker GK, Wang Z, Wolf AB, Xu K-M, Yang F, Zhang G. 2009. Intercomparison of model simulations of mixed-phase clouds observed during the ARM Mixed-Phase Arctic Cloud Experiment. I: multilayer cloud. *Quarterly Journal of the Royal Meteorological Society* **135**: 1003–1019.
- NASA. 2011. ICESat mission status report. <http://icesat.gsfc.nasa.gov/icesat/> (updated 21 January 2011).
- Neely RR III, Thayer JP. 2010. Initial results from ARCLITE tropospheric water vapor profiling and balloon validation. *Proceedings of 25th International Laser Radar Conference*, St. Petersburg; 1195–1197.
- Neely RR III, Thayer JP, Hardesty RM, Hayman M, O'Neill M, Eberhard W, Alvarez RJ, Marchbanks R, Sandberg S. 2010. Depolarization lidar at summit, Greenland for the detection of cloud phase and stratospheric aerosols. *Proceedings of 25th International Laser Radar Conference*, St. Petersburg; 453–456.
- Noel V, Chepfer H. 2010. A global view of horizontally oriented crystals in ice clouds from Cloud-Aerosol Lidar and Infrared Pathfinder Satellite Observation (CALIPSO). *Journal of Geophysical Research* **115**: D00H23, DOI: 10.1029/2009JD012365.
- Noel V, Sassen K. 2005. Study of planar ice crystal orientations in ice clouds from scanning polarization lidar observations. *Journal of Applied Meteorology* **44**: 653–664.
- Noel V, Winker DM, McGill M, Lawson P. 2004. Classification of particle shapes from lidar depolarization ratio in convective ice clouds compared to in situ observation during CRYSTAL-FACE. *Journal of Geophysical Research* **109**: D24213, DOI: 10.1029/2004JD004883.
- Nott GJ, Duck TJ, Doyle JG, Coffin MEW, Perro C, Thackray CP, Drummond JR, Fogal PF, McCullough E, Sica RJ. 2011. A remotely-operated lidar for aerosol, temperature, and water vapor profiling in the High Arctic. *Journal of Atmospheric and Oceanic Technology* (submitted).
- Olofson KFG, Svensson EA, Witt G, Pettersson JBC. 2009. Arctic aerosol and clouds studied by bistatic lidar technique. *Journal of Geophysical Research* **114**: D18208, DOI: 10.1029/2008JD011138.
- Palm SP, Strey ST, Spinhirne J, Markus T. 2010. Influence of Arctic sea ice extent on polar cloud fraction and vertical structure and implications for regional climate. *Journal of Geophysical Research* **115**: D21209, DOI: 10.1029/2010JD013900.
- Pietruczuk A, Karasiński G. 2010. Lidar at Polish polar station, instrument design and first results. *Proceedings of 25th International Laser Radar Conference*, St. Petersburg; 163–165.
- Pitts MC, Poole LR, Thomason LW. 2009. CALIPSO polar stratospheric cloud observations: second-generation detection algorithm and composition discrimination. *Atmospheric Chemistry and Physics* **9**: 7577–7589.
- Quinn PK, Miller TL, Bates TS, Ogren JA, Andrews E, Shaw GE. 2002. A 3-year record of simultaneously measured aerosol chemical and optical properties at Barrow, Alaska. *Journal of Geophysical Research* **107**: D11, DOI: 10.1029/2001JD001248.
- Quinn PK, Shaw G, Andrews E, Dutton EG, Ruoho-Airola T, Gong SL. 2007. Arctic haze: current trends and knowledge gaps. *Tellus* **59B**: 99–114.
- Radke LF, Brock CA, Lyons JH, Hobbs PV, Schnell RC. 1989. Aerosol and lidar measurements of hazes in mid-latitude and polar airmasses. *Atmospheric Environment* **23**: 2417–2430.
- Randall D, Curry J, Battisti D, Flato G, Grumbine R, Hakkinen S, Martinson D, Preller R, Walsh J, Weatherly J. 1998. Status of and outlook for large-scale modeling of atmosphere-ice-ocean interactions in the Arctic. *Bulletin of the American Meteorological Society* **79**: 197–219.
- Randel DL, Vonder Haar TH, Ringerud MA, Stephens GL, Greenwald TJ, Combs CL. 1996. A new global water vapor dataset. *Bulletin of the American Meteorological Society* **77**: 1233–1246.
- Rangno AL, Hobbs PV. 2001. Ice particles in stratiform clouds in the Arctic and possible mechanisms for the production of high ice concentrations. *Journal of Geophysical Research* **106**: 15065–15075.
- Rauber RM, Tokay A. 1991. An explanation for the existence of supercooled water at the top of cold clouds. *Journal of Atmospheric Sciences* **48**: 1005–1023.
- Ridley BA, Atlas EL, Montzka DD, Browell EV, Cantrell CA, Blake DR, Blake NJ, Cinquini L, Coffey MT, Emmons LK, Cohen RC, DeYoung RJ, Dibb JE, Eisele FL, Flocke FM, Fried A, Grahek FE, Grant WB, Hair JW, Hannigan JW, Heikes BJ, Lefer BL, Mauldin RL, Moody JL, Shetter RE, Snow JA, Talbot RW, Thornton JA, Walega JG, Weinheimer AJ, Wert BP, Wimmers AJ. 2003. Ozone depletion events observed in the high latitude surface layer during the TOPSE aircraft program. *Journal of Geophysical Research* **108**: 8356, DOI: 10.1029/2001JD001507.
- Sacco VM, Castagnoli F, Morandi M, Stefanutti L. 1989. Elastic backscattering lidar system for atmospheric measurements in Antarctica. *Optical and Quantum Electronics* **21**: 215–226.
- Santacesaria V, MacKenzie AR, Sefanutti L. 2001. A climatological study of polar stratospheric clouds (1989–1997) from LIDAR measurements over Dumont d'Urville (Antarctica). *Tellus* **53B**: 306–321.
- Santacesaria V, Stefanutti L, Morandi M, Guzzi D, MacKenzie AR. 1999. Two-year (1996/1997) ozone DIAL measurement over

- Dumont d'Urville (Antarctica). *Geophysical Research Letters* **26**: 463–466.
- Sassen K. 2005. Polarization in lidar. In *Lidar: Range-Resolved Optical Remote Sensing of the Atmosphere*, Weitkamp C (ed.). Springer: Singapore; 19–42.
- Sassen K, Zhu J. 2009. A global survey of CALIPSO linear depolarization ratios in ice clouds: initial findings. *Journal of Geophysical Research* **114**: D00H07, DOI: 10.1029/2009JD012279.
- Schnell RC, Barry RG, Miles MW, Andreas EL, Radke LF, Brock CA, McCormick MP, Moore JL. 1989. Lidar detection of leads in Arctic sea ice. *Nature* **339**: 530–532.
- Shiobara M, Yabuki M, Kobayashi H. 2003. A polar cloud analysis based on micropulse lidar measurements at Ny-Ålesund, Svalbard and Syowa, Antarctica. *Physics and Chemistry of the Earth* **28**: 1205–1212.
- Shiple ST, Tracy DH, Eloranta EW, Trauger JT, Sroga JT, Roesler FL, Weinman JA. 1983. High spectral resolution lidar to measure optical scattering properties of atmospheric aerosols. 1: theory and instrumentation. *Applied Optics* **22**: 3716–3724.
- Shupe MD, Daniel JS, de Boer G, Eloranta EW, Kollias P, Long CN, Luke EP, Turner DD, Verlinde J. 2008b. A focus on mixed phase clouds. The status of ground-based observational methods. *Bulletin of the American Meteorological Society* **89**: 1549–1562.
- Shupe MD, Kollias P, Persson POG, McFarquhar GM. 2008a. Vertical motions in Arctic mixed-phase stratiform clouds. *Journal of Atmospheric Sciences* **65**: 1304–1322.
- Shupe MD, Intrieri JM. 2004. Cloud radiative forcing of the Arctic surface: the influence of cloud properties, surface albedo, and solar zenith angle. *Journal of Climate* **17**: 616–628.
- Shupe MD, Matrosov SY, Uttal T. 2005. Arctic mixed-phase cloud properties derived from surface-based sensors. *Fifteenth ARM Science Team Meeting Proceedings*, Daytona Beach, Florida. Atmospheric Radiation Measurement Program, U.S. Department of Energy. <http://www.arm.gov/publications/proceedings/conf15/> (accessed 7 August 2011).
- Sikand M, Koskulics J, Stamnes K, Hamre B, Stamnes J, Lawson R. 2010. Optical properties of mixed phase boundary layer clouds observed from a tethered balloon platform in the Arctic. *Journal of Quantitative Spectroscopy and Radiative Transfer* **111**: 1921–1930.
- Simpson WR, von Glasow R, Riedel K, Anderson P, Ariya P, Bottenheim J, Burrows J, Carpenter LJ, Frieß U, Goodsite ME, Heard D, Hutterli M, Jacobi H-W, Kaleschke L, Neff B, Plane J, Platt U, Richter A, Roscoe H, Sander R, Shepson P, Sodeau J, Steffen A, Wagner T, Wolff E. 2007. Halogens and their role in polar boundary-layer ozone depletion. *Atmospheric Chemistry and Physics* **7**: 4375–4418.
- Smiley VN, Morley BM. 1981. Lidar depolarization studies of the atmosphere at the South Pole. *Applied Optics* **20**: 2188–2195.
- Smiley VN, Morley BM, Warburton JA. 1979. Lidar operations at Palmer Station. *Antarctic Journal of the United States* **14**: 205–206.
- Smiley VN, Warburton JA, Morley BM. 1975. South Pole ice crystal precipitation studies using lidar sounding and replication. *Antarctic Journal of the United States* **10**: 230–231.
- Soden BJ, Held IM. 2006. An assessment of climate feedbacks in coupled ocean-atmosphere models. *Journal of Climate* **19**: 3354–3360.
- Spinhirne JD, Palm SP, Hart WD. 2005. Antarctica cloud cover for October 2003 from GLAS satellite lidar profiling. *Geophysical Research Letters* **32**: L22S05, DOI: 10.1029/2005GL023782.
- Stachlewska IS, Neuber R, Lampert A, Ritter C, Wehrle G. 2010. AMALi – the airborne mobile aerosol lidar for Arctic research. *Atmospheric Chemistry and Physics* **10**: 2947–2963.
- Stefanutti L, Castagnoli F, Del Guasta M, Morandi M, Sacco VM, Zuccagnoli L, Godin S, Megie G, Porteneuve J. 1992b. The Antarctic ozone LIDAR system. *Applied Physics B* **55**: 3–12.
- Stefanutti L, Castagnoli F, Del Guasta M, Morandi M, Sacco VM, Venturi V, Zuccagnoli L, Kolenda J, Kneipp H, Rairoux P, Stein B, Weidauer D, Wolf JP. 1992a. A four-wavelength depolarization backscattering LIDAR for polar stratospheric cloud monitoring. *Applied Physics B* **55**: 13–17.
- Stone RS, Herber A, Vitale V, Mazzola M, Lupi A, Schnell RC, Dutton EG, Liu PSK, Li S, Dethloff K, Lampert A, Ritter C, Stock M, Neuber R, Maturilli M. 2010. A three-dimensional characterization of Arctic aerosols from airborne Sun photometer observations: PAMARCMIP, April 2009. *Journal of Geophysical Research* **115**: D13203, DOI: 10.1029/2009JD013605.
- Strawbridge KB, Snyder BJ. 2001. Daytime and nighttime aircraft lidar measurements showing evidence of particulate matter transport into the Northeastern valleys of the Lower Fraser Valley, BC. *Atmospheric Environment* **38**: 1352–2310.
- Tao Z, McCormick MP, Wu D, Liu Z, Vaughan MA. 2008. Measurements of cirrus cloud backscatter color ratio with a two-wavelength lidar. *Applied Optics* **47**: 1478–1485.
- Thayer JP, Nielsen NB, Warren RE, Heinselman CJ, Sohn J. 1997. Rayleigh lidar system for middle atmosphere research in the arctic. *Optical Engineering* **36**: 2045–2061.
- Tomasi C, Vitale V, Lupi A, Di Carmine C, Campanelli M, Herber A, Treffeisen R, Stone RS, Andrews E, Sharma S, Radionov V, von Hoyningen-Huene W, Stebel K, Hansen GH, Myhre CL, Wehrli C, Aaltonen V, Lihavainen H, Virkkula A, Hillamo R, Ström J, Toledano C, Cachorro VE, Ortiz P, de Frutos AM, Blindheim S, Frioud M, Gausa M, Zielinski T, Petelski T, Yamanouchi T. 2007. Aerosols in polar regions: a historical overview based on optical depth and in situ observations. *Journal of Geophysical Research* **112**: D16205, DOI: 10.1029/2007JD008432.
- Turner DD. 2005. Arctic mixed-phase cloud properties from AERI lidar observations: algorithm and results from SHEBA. *Journal of Applied Meteorology* **44**: 427–444.
- Turner DD, Goldsmith JEM. 1999. Twenty-four-hour Raman lidar water vapor measurements during the atmospheric radiation measurement program's 1996 and 1997 water vapor intensive observation periods. *Journal of Atmospheric and Oceanic Technology* **16**: 1062–1076.
- Uttal T, Curry JA, McPhee MG, Perovich DK, Moritz RE, Maslanik JA, Guest PS, Stern HL, Moore JA, Turenne R, Heiberg A, Serreze MC, Wylie DP, Persson OG, Paulson CA, Halle C, Morison JH, Wheeler PA, Makstas A, Welch H, Shupe MD, Intrieri JM, Stamnes K, Lindsey RW, Pielke R, Pegau WS, Stanton TP, Grenfeld TC. 2002. Surface heat budget of the Arctic Ocean. *Bulletin of the American Meteorological Society* **83**: 255–276.
- Vaughan G, Warfing DP, Thomas L, Mitev V. 1988. Humidity measurements in the free troposphere using Raman backscatter. *Quarterly Journal of the Royal Meteorological Society* **114**: 1471–1484.
- Verlinde J, Harrington JY, Yannuzzi VT, Avramov A, Greenberg S, Richardson SJ, Bahrman CP, McFarquhar GM, Zhang G, Johnson N, Poellot MR, Mather JH, Turner DD, Eloranta EW, Tobin DC, Holz R, Zak BD, Ivey MD, Prenni AJ, DeMott PJ, Daniel JS, Kok GL, Sassen K, Spangenberg D, Minnis P, Tooman TP, Shupe M, Heymsfield AJ, Schofield R. 2007. The mixed-phase Arctic cloud experiment. *Bulletin of the American Meteorological Society* **88**: 205–221.
- de Villiers RA, Ancellet G, Pelon J, Quennehen B, Schwarzenboeck A, Gayet JF, Law KS. 2010. Airborne measurements of aerosol optical properties related to early spring transport of mid-latitude sources into the Arctic. *Atmospheric Chemistry and Physics* **10**: 5011–5030.
- Walden VP, Warren SG, Tuttle E. 2003. Atmospheric ice crystals over the Antarctic Plateau in winter. *Journal of Applied Meteorology* **42**: 1391–1405.
- Walsh JE, Chapman WL. 1998. Arctic cloud-radiation-temperature associations in observational data and atmospheric reanalyses. *Journal of Climate* **11**: 3030–3045.
- Weitkamp C. (ed.) 2005. *Lidar: Range-Resolved Optical Remote Sensing of the Atmosphere*. Springer: Singapore.
- Wendling P, Wendling R, Renger W, Covert D, Heintzenberg J, Moerl P. 1985. Calculated radiative effects of Arctic haze during a pollution episode in Spring 1983 based on ground-based and airborne measurements. *Atmospheric Environment* **19**: 2181–2193.
- Wessel S, Aoki S, Winkler P, Weller R, Herber A, Gernandt H. 1998. Tropospheric ozone depletion in polar regions a comparison of observations in the Arctic and Antarctic. *Tellus* **50B**: 34–50.
- Westbrook CD, Illingworth AJ, O'Connor EJ, Hogan RJ. 2010. Doppler lidar measurements of oriented planar ice crystals falling from supercooled and glaciated layer clouds. *Quarterly Journal of the Royal Meteorological Society* **136**: 260–276.
- Winker DM, Vaughan MA, Omar A, Hu Y, Powell KA, Liu Z, Hunt WH, Young SA. 2009. Overview of the CALIPSO mission and CALIOP data processing algorithms. *Journal of Atmospheric and Oceanic Technology* **26**: 2310–2323.
- Wirth M, Fix A, Mahnke P, Schwarzer H, Schrandt F, Ehret G. 2009. The airborne multi-wavelength water vapor differential absorption lidar WALEs: system design and performance. *Applied Physics B* **96**: 201–213.

- Wyser K, Jones CG. 2005. Modeled and observed clouds during Surface Heat Budget of the Arctic Ocean (SHEBA). *Journal of Geophysical Research* **110**: D09207, DOI: 10.1029/2004JD004751.
- Yamanouchi T, Treffeisen R, Herber A, Shiobara M, Yamagata S, Hara K, Sato K, Yabuki M, Tomikawa Y, Rinke A, Neuber R, Schumacher R, Kriews M, Ström J, Schrems O, Gernandt H. 2005. Arctic study of tropospheric aerosol and radiation (ASTAR) 2000: arctic haze case study. *Tellus* **57B**: 141–152.
- Yoshida R, Okamoto H, Hagihara Y, Ishimoto H. 2010. Global analysis of cloud phase and ice crystal orientation from Cloud-Aerosol Lidar and Infrared Pathfinder Satellite Observation (CALIPSO) data using attenuated backscattering and depolarization ratio. *Journal of Geophysical Research* **115**: D00H32, DOI:10.1029/2009JD012334.
- von Zahn U, von Cossart G, Fiedler J, Fricke KH, Nelke G, Baumgarten G, Rees D, Hauchecorne A, Adolfsen K. 2000. The ALOMAR Rayleigh/Mie/Raman lidar: objectives, configuration, and performance. *Annales Geophysicae* **18**: 815–833.
- Zuidema P, Baker B, Han Y, Intrieri J, Key J, Lawson P, Matrosov S, Shupe M, Stone R, Uttal T. 2005. An Arctic springtime mixed-phase cloudy boundary layer observed during SHEBA. *Journal of Atmospheric Sciences* **62**: 160–176.